catalysts

MDPI

Review

Visible-Light-Active TiO_2-Based Hybrid Nanocatalysts for Environmental Applications

Alessandra Truppi [1,2], Francesca Petronella [1], Tiziana Placido [1], Marinella Striccoli [1], Angela Agostiano [1,2], Maria Lucia Curri [1] and Roberto Comparelli [1,*]

[1] CNR-IPCF, Istituto Per i Processi Chimici e Fisici, U.O.S. Bari, c/o Dip. Chimica Via Orabona 4, 70126 Bari, Italy; a.truppi@ba.ipcf.cnr.it (A.T.); f.petronella@ba.ipcf.cnr.it (F.P.); t.placido@ba.ipcf.cnr.it (T.P.); m.striccoli@ba.ipcf.cnr.it (M.S.); angela.agostiano@chimica.uniba.it (A.A.); lucia.curri@ba.ipcf.cnr.it (M.L.C.)

[2] Dipartimento di Chimica Università degli Studi di Bari "A. Moro", Via Orabona 4, 70126 Bari, Italy

* Correspondence: roberto.comparelli@cnr.it; Tel.: +39-80-544-2027

Academic Editors: Shaobin Wang and Xiaoguang Duan
Received: 20 January 2017; Accepted: 22 March 2017; Published: 25 March 2017

Abstract: Photocatalytic nanomaterials such as TiO_2 are receiving a great deal of attention owing to their potential applications in environmental remediation. Nonetheless, the low efficiency of this class of materials in the visible range has, so far, hampered their large-scale application. The increasing demand for highly efficient, visible-light-active photocatalysts can be addressed by hybrid nanostructured materials in which two or more units, each characterised by peculiar physical properties, surface chemistry and morphology, are combined together into a single nano-object with unprecedented chemical–physical properties. The present review intends to focus on hybrid nanomaterials, based on TiO_2 nanoparticles able to perform visible-light-driven photocatalytic processes for environmental applications. We give a brief overview of the synthetic approaches recently proposed in the literature to synthesise hybrid nanocrystals and discuss the potential applications of such nanostructures in water remediation, abatement of atmospheric pollutants (including NO_x and volatile organic compounds (VOCs)) and their use in self-cleaning surfaces.

Keywords: photocatalysis; titanium dioxide; nanomaterials; heterostructures; visible light; sunlight; environmental remediation; organic pollutants; NO_x; VOCs; self-cleaning surfaces

1. Introduction

Visible-light-driven photocatalytic processes represent the current frontier of research in the field of photocatalysis. Indeed, in spite of the great deal of attention devoted to photoactive nanomaterials in the last 20 years, their scarce efficacy under solar light and, thus, the high cost of the photocatalytic processes, has still hampered their large-scale application [1–4].

Semiconductor-assisted photocatalytic oxidation processes can be potentially exploited in photocatalysis, air and water remediation, self-cleaning and bactericidal coatings, new generation solar cells, hydrogen production, sensing and cultural heritage protection [2,4–11]. TiO_2 has been regarded as among the most promising materials, owing to its high chemical stability, commercial availability and outstanding photocatalytic activity [3]. Nanosized TiO_2 demonstrated improved performances, with respect to its bulk counterpart, thanks to its extremely high surface-to-volume ratio that turns into a high density of catalytically active surface sites [12–14]. In addition, thanks to the size-dependent band gap of nanosized semiconductors, it is possible to finely tune the redox potentials of photogenerated electron–hole pairs to selectively control photochemical reactions. Furthermore, charges photogenerated in nanocatalysts can easily reach the catalyst surface, thus decreasing the probability of bulk recombination [3,15]. As a drawback, because of its large band gap (3.2 eV), the absorption onset of bare TiO_2 falls in the UV, thus resulting in a low efficiency for visible or

sunlight-driven photocatalytic applications. Indeed, the UV fraction of the solar spectrum is only ~4%, whereas the proportion of photons in the visible region reaches nearly 50% [16]. Therefore, effective harvest of such a highly intense photon flux portion would represent a remarkable breakthrough toward the large-scale application of photocatalysis, ultimately addressing the growing demand of clean industrial processes. An additional challenge is represented by the need to improve the efficiency of photocatalytic processes in order to reduce electron–hole (e^-/h^+) pair recombination, and to finely control size, shape, crystalline phase and surface chemistry of TiO_2 nanoparticles.

Indeed, the capability to tune size and shape allows us to increase the surface-to-volume ratio (i.e., the density of catalytically active surface sites) and to tailor the redox potential e^-/h^+ pairs and expose selected crystalline planes [17]. In general, the strategies proposed to increase the lifetime of e^-/h^+ and improve the photoactivity of TiO_2 in the visible range can be classified as follows: (i) introduction of red-ox couples or noble metals at semiconductor particle surface; (ii) doping with metal of non-metal atoms; (iii) coupling with narrow band gap semiconductors able to absorb visible light. Among the plethora of approaches proposed in the literature so far [1,2,18–20], hybrid nanocrystals, i.e., nanostructured materials formed by two or more components, each characterised by peculiar physical properties, surface chemistry and morphology, combined together into one nano-object, hold great promise for the development of multifunctional nanocatalysts. Indeed, hybrid nanocrystals offer the opportunity to merge in one material photocatalytic semiconductors and plasmonic structures, or semiconductors and oxides with a different energy gap, or semiconducting and magnetic oxides, resulting in countless possible combinations [2,18,20–25]. Besides the photoactivity under visible light irradiation, hybrid nanocrystals could also provide spatial separation of e^-/h^+, thus improving the lifetime of the excited state and an opportunity to magnetically recover the photocatalysts or activate biocidal function even in the dark.

In the present review, we will focus our attention on such a class of hybrid nanocrystals, able to perform visible-light-driven photocatalytic processes for environmental application. In the first section, we give a brief overview of the synthetic approaches for their preparation, mainly focusing on wet chemical syntheses. In the second part of the review, we will discuss the potential application of hybrid nanocrystals in water remediation, abatement of atmospheric pollutants (NO_x and volatile organic compounds (VOCs)) and their integration in construction materials for achieving self-cleaning surfaces and photocatalytic cements.

2. Synthesis

Solution-based techniques for the preparation of hybrid nanocrystals exploit the well-known principle of the Classical Nucleation Theory, which considers that the activation energy for the generation of a particle in solution (homogeneous nucleation) is much higher than the energy required to enlarge a pre-existing particle (heterogeneous nucleation) [22]. Indeed, the general reaction scheme starts from preformed nanocrystals of one material, which act as a "seed" for the nucleation of the second material. Usually, such seeds are already present or they are introduced into the reaction vessel containing the molecular precursors of the second, different material. Colloidal bottom-up routes are widely employed for this purpose because they allow nanometric shape control and, at the same time, preserve the chemical–physical identity of each component, thus maximizing the resulting synergistic properties. Such a goal can be accomplished by setting the reaction conditions in order to promote the heterogeneous growth of a new material on the pre-formed "seed particle", instead of enabling the homogenous formation of new particles. The features of the seed particles, including size, shape and faceting, can affect the morphology of the resulting heterostructures. Indeed, in principle, a low interfacial energy between the two materials results in a core shell geometry, while large interfacial energy gives rise to heterodimers. Remarkably, when the "seed particle" has rod-like geometry, it is possible to exploit the different reactivity of the rod facets in order to grow a second material on a selected facet [23,26].

In this section, we give a brief overview of synthetic approaches for photoactive hybrid nanocrystals, addressing the reader to more specific reviews for a deeper discussion [18,21,22].

2.1. TiO_2/Semiconductor Hybrid Nanocrystals

In recent years, the combination of TiO_2 nanomaterials with other semiconductors has been demonstrated to be very promising in enhancing photocatalytic activity. In particular, the coupling of TiO_2 with semiconductors with different band gaps has been proposed to extend the absorption wavelength range to the visible range and to hamper the e^+/h^+ recombination [27,28]. The TiO_2/semiconductors hybrid heterostructures can be divided into: p-n semiconductor heterojunction and non-p-n heterojunction systems. When p- and n-type semiconductors come into contact, a so-called "space-charge region" is generated at the interface, thus forming a p-n junction. In the "space-charge region" a charge density depletion occurs, thus creating "built-in potential"—that is, a difference of potential able to drive the charge carriers to travel in the opposite direction. These systems, including Cu_2O/TiO_2 [29], $CuBi_2O_4/TiO_2$ [30], NiS/TiO_2 [31], and Graphene Oxide/TiO_2 [32], show several advantages: (1) improved charge separation; (2) improved charge transfer to the catalyst; and (3) longer charge carrier lifetime. On the other hand, in non-p-n heterojunctions, the two semiconductors (A and B) are tightly bound to build an efficient heterostructure in which the internal field is able to promote the separation and migration of photogenerated carriers. For such non-p-n heterojunction systems, like CdS/TiO_2 [33], InO_3/TiO_2 [34], WO_3/TiO_2 [35], Fe_2O_3/TiO_2 [36], and ZnO/TiO_2 [24,25] the staggered band gap type structure is the most suitable for photocatalytic applications [27].

Generally speaking, visible-light-active TiO_2-based hybrid heterostructures based on coupled semiconductors are a combination of TiO_2 with a second semiconductor nanoparticle with a narrower band gap able to generate an e^-/h^+ pair upon irradiation with visible light, so that the electrons can migrate towards the TiO_2 conduction band, while holes are trapped in the second material (Figure 1) [37]. Notably, hybrid nanocrystals can be rationally designed in order to produce a favourable alignment of band offset and energy levels.

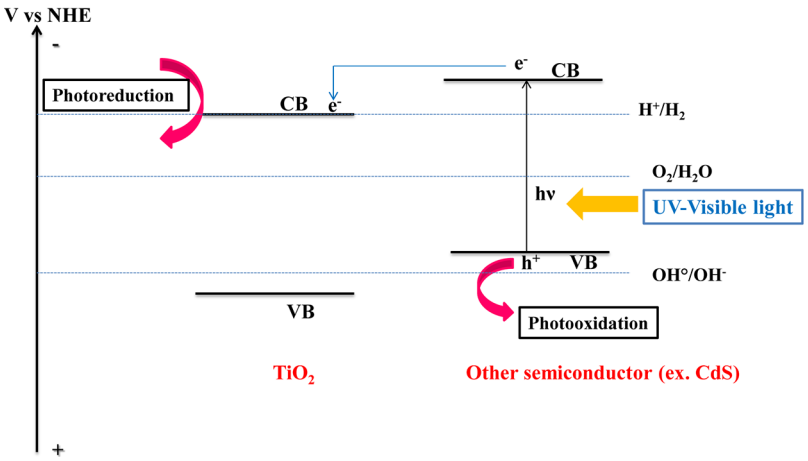

Figure 1. Pictorial representation of electron−holes (e^-/h^+) transfer in a coupled semiconductor system. Reprinted with permission from [28]. Copyright 2013, American Chemical Society.

The photocatalytic performance of these coupled semiconductors is related to the geometry of the particles, the extent of contact surface between particles and the particle size, besides the flat band potential of the components. These parameters strongly depend on the method used for their preparation [1]. Moreover, the coupling may occur in many forms such as layered or core-shell structures and various fabrication methods can be applied, including chemical synthesis, solution- or gas-phase deposition, and templated fabrication [37]. Coupled oxide-based hybrid

nano-heterostructures (M_xO_y/TiO_2) and sulphide-based nano-heterostructures M_xS_y/TiO_2 are the most widely used to improve visible-irradiation-driven photocatalytic processes [28].

2.1.1. M_xO_y/TiO_2-Based Hybrid Nanocrystals

TiO_2 containing visible-light-active nanosized heterostructures based on coupled oxides generally exploit oxide semiconductors with a band gap energy lower than that of TiO_2 and with a more negative redox potential of conduction band (CB) electrons in order to absorb visible light and inject photo-generated electrons in TiO_2 CB. Under these conditions, the CB electrons in TiO_2 can initiate the photoreduction processes responsible for pollutant removal.

In particular, the TiO_2/WO_3 couple has received much attention for improving the photocatalytic properties of TiO_2 under visible light irradiation, since WO_3 can be regarded as an electron accepting species. Indeed, both valence and conduction band of WO_3 lie below those of TiO_2. In addition, WO_3 has a narrow band gap (~2.8 eV). Therefore, under visible light, photogenerated electrons can be excited from the valence band (VB) to the CB of WO_x and the holes in the VB of WO_x can be transferred to TiO_2 or remain in the VB of WO_x (Figure 2) [28].

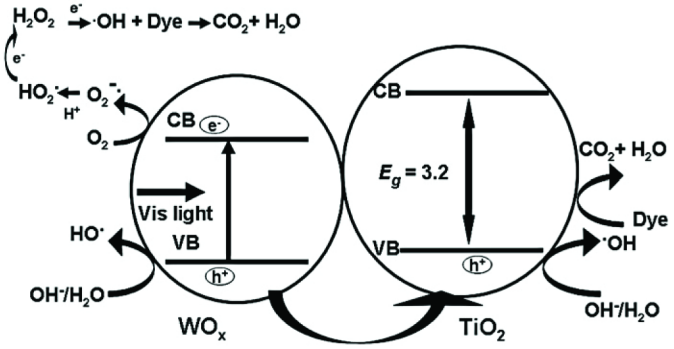

Figure 2. Suggested mechanism of dye degradation in visible light by a WO_x/TiO_2 composite. Reprinted with permission from [38]. Copyright 2010, Elsevier.

Sajjad et al. synthesised WO_3/TiO_2 by a sol-gel process using solutions of $Ti(OBu)_4$ and solutions of ammonium tungstate. Subsequently, the product was activated in a single-step thermal treatment in a vacuum to enhance the photocatalytic activity in the visible region [38]. Recently, Ren et al. prepared TiO_2/WO_3 composites with different contents of tungsten oxide by a microwave-assisted hydrothermal method, an environmentally friendly and novel process. Specifically, they have prepared TiO_2/WO_3 from $TiCl_4$ and Na_2WO_4 without using any organic species [35].

Furthermore, a promising strategy to enhance the visible-light photocatalytic performance is to combine Bi_2WO_6 with TiO_2. The photocatalyst based on the TiO_2/Bi_2WO_6 heterojunction has been synthesised by a simple and practical liquid phase method [39]. The hybrid nanocrystals are characterised by a special morphology with the TiO_2 particles coating the surface of the flower-like Bi_2WO_6 microspheres. The obtained heterostructure has demonstrated improved light harvesting efficiency and effective electron/hole pair separation, which results in improved photoactivity.

Also, $BiFeO_3/TiO_2$ and $ZnFeO_4/TiO_2$ are favourable materials to develop a high-efficiency photocatalyst active in the visible region [1]. Core-shell structured $BiFeO_3/TiO_2$ nanocomposites have been synthesised by a hydrothermal process, followed by hydrolysis precipitation of tetrabutyl titanate (TBOT). The results indicate that $BiFeO_3/TiO_2$ nanocomposites have good visible-light absorption properties, which should be induced by Fe or Bi/Ti interdiffusion in the interfaces [40]. $ZnFeO_4/TiO_2$-coupled semiconductors have been successfully fabricated by a two-step process of anodization and a vacuum-assisted impregnation method, followed by annealing. In this case, the $ZnFe_2O_4$ sensitization enhances the probability of photoinduced charge separation and extends the range of the photoresponse of TiO_2 nanotube arrays from the UV to the visible region [41].

Hybrid nanocrystals based on one-dimensional (1D) TiO_2 nanofibres have attracted increased attention because of their large surface area and reduced diffusion length compared to conventional TiO_2-based materials. Considerable attention has recently been devoted to In_2O_3 as a co-catalyst in the formation of hybrid heterostructures with TiO_2. A rich variety of In_2O_3–TiO_2 photocatalysts has been prepared, including nanoparticles, films, and so on. Mu et al. fabricated a one-dimensional In_2O_3–TiO_2 architecture based on TiO_2 nanofibers by combining the electrospinning technique with the solvothermal method. Furthermore, the In_2O_3–TiO_2 heterostructures fabricated as nanofibres could be easily recycled without a decrease in the photocatalytic activity (Figure 3) [34].

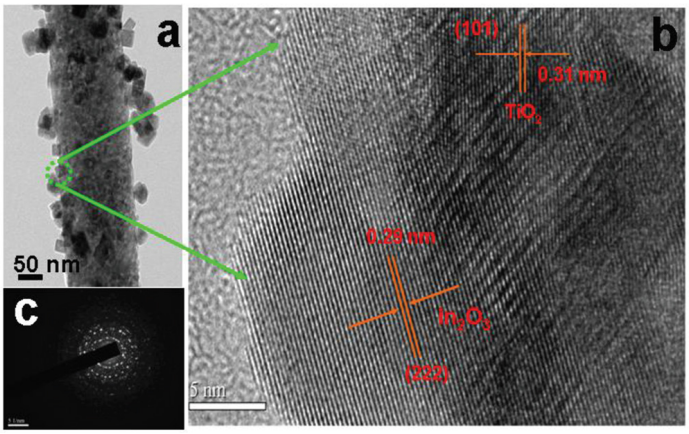

Figure 3. In_2O_3–TiO_2 heteroarchitecture sample (with 15% mass percentage of In_2O_3): (**a**) Transmission electron microscopy (TEM) image; (**b**) High-resolution TEM (HRTEM) image; (**c**) Selected area electron diffraction (SAED) pattern. Reprinted with permission from [34]. Copyright 2012, American Chemical Society.

Recently, other architectures have been considered as well, including Cu_2O deposited on TiO_2 nanowires, Cu_2O on TiO_2 nanosheets, and Cu_2O/TiO_2 core-shell structures, all showing improved photocatalytic performance under visible light when compared to pure TiO_2 [37]. Bi et al. synthesised Cu_2O hollow nanospheres combined with TiO_2 through in situ hydrolysis of $Ti(OBu)_4$ under sonication. In this case, the formation of a p-n heterojunction in the composites induces an efficient suppression of recombination of the photogenerated electrons and holes, as well as the enhanced stability of the catalyst and, thereby, the improved visible-light photocatalytic activity [42].

2.1.2. M_xS_y/TiO_2-Based Hybrid Nanocrystals

The coupling of CdS and TiO_2 nanoparticles has attracted great attention due to the ability of CdS, upon visible light excitation, to promote electrons in the conduction band, which can subsequently be injected into the TiO_2 conduction band. Liu et al. reported a facile, template-free synthesis of CdS/TiO_2 core-shell hybrid nanocrystals via a two-step solvothermal method. A uniform layer of TiO_2 has been deposited onto the CdS core, thus forming the CdS core/TiO_2 shell semiconductor nanocomposites [43].

Another example is CdS/TiO_2 nanofibres, which have been synthesised by a simple and practical electrospinning-assisted route. Specifically, CdS nanoparticles have been dispersed within the entire surface of the as electrospun TiO_2 nanofibers, forming hierarchical hybrid nanocrystals. Compared with P25 and the unmodified TiO_2 nanofibers, the CdS/TiO_2 nanofibers have exhibited enhanced photocatalytic activity under visible-light irradiation, which might arise from the increased surface area and the promoted electrons–holes separation on the hierarchical structure (Figure 4) [44].

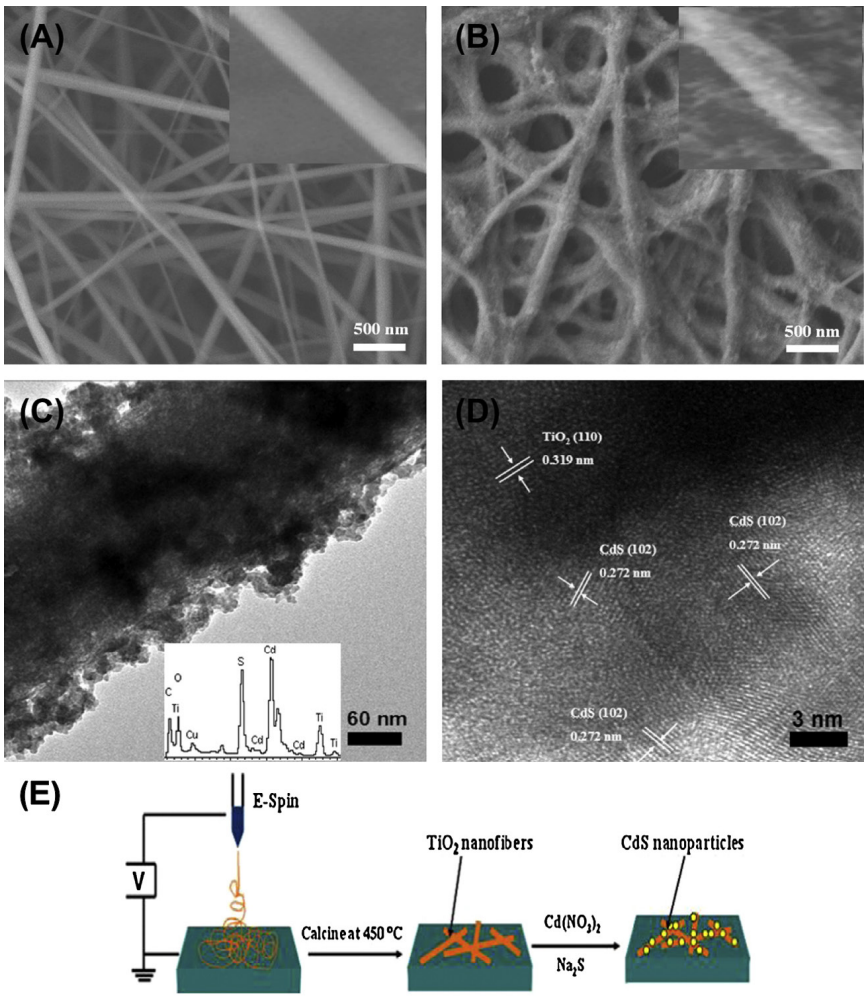

Figure 4. Scanning electron microscope (SEM) images of (**A**) the prepared TiO_2 nanofibres and (**B**) CdS modified TiO_2 nanofibres. Insets show the corresponding individual nanofibre; (**C**) TEM image of the as electrospun TiO_2 nanofibres. The inset shows the Energy-dispersive X-ray spectroscopy (EDS) analysis of the sample; (**D**) HRTEM of CdS/TiO_2 nanofibres; (**E**) Schematic illustration of the formation mechanism of CdS modified TiO_2 nanofibres. Reprinted with permission from [44]. Copyright 2014, Elsevier.

CuS has been also regarded as a possible alternative to CdS to convey photocatalytic activity in the visible light range to TiO_2 nanoparticles. As an example, Fe-doped TiO_2 nanotubes have been decorated with CuS nanoparticles. In the first step, Fe-doped TiO_2 (Fe:/TiO_2) nanotubes have been synthesised by means of a sol-gel process involving the hydrothermal reaction of butyltitanate and ferric nitrate. Subsequently, CuS nanoparticles have been grown on the surface of Fe:TiO_2 nanotubes by successive ionic adsorption and a reaction method. Under constant ultrasonication, drops of Cu^{2+} and of S^{2-} precursor solution have been alternatively added to the dispersion of the Fe:TiO_2 nanotubes. The obtained heterostructures have demonstrated improved photocatalytic performance under solar irradiation for the degradation of malachite green and naphthol green B [45]. Recently, CuS nanoflowers, fabricated by an element-direct-reaction route by using copper and sulphur powder, have been loaded on rutile TiO_2 nanoparticles, demonstrating the ability to photocatalyze the degradation of methylene blue and 4-chlorophenol upon irradiation in the visible range [46].

Currently, the ternary chalcogenides, such as $AgInS_2$, represent an emerging class of materials that can be successfully combined with TiO_2, due to their excellent catalytic performance and the wide optical response in the visible range. Liu et al. have reported that $AgInS_2$/TiO_2 composites

synthesised by a one-pot hydrothermal method have exhibited enhanced photoactivity under visible light compared to TiO_2 P25 as a reference material. The photocatalytic performance has been discussed in terms of the quantum calculation of $AgInS_2$ and the proper band alignment in the $AgInS_2/TiO_2$ composites. The hybrid nanocrystals show a band gap of 2.75 eV, in good agreement with the density of state calculations. According to surface photovoltage spectra, the heterostructures are expected to be efficient in separating the photogenerated electron and hole pairs [47].

2.2. TiO_2/Plasmonic Material-Based Hybrid Nanocrystals

To go beyond the limited photocatalytic efficiency of pure TiO_2 under solar light due to its large band gap (3.2 eV), a new method for harvesting visible light has emerged, involving the strong plasmon resonance of Ag and Au nanoparticles [48]. Surface plasmons are the collective oscillation of the free charges confined to the surfaces of a noble metal. Metal nanoparticles, when irradiated with light at their plasmon frequency, generate intense electric fields at their surface. The frequency of this resonance depends on the nanoparticle size, shape, chemical composition and proximity to other nanoparticles. Therefore, control of such parameters allows us to tune the position of the plasmon absorbance band in the whole Vis-NIR (Near-Infrared) range [48–52]. In particular, in an anisotropic nanoparticle, such as a nanorod (NR), the oscillation of electrons could occur along the transverse and longitudinal axis, thus splitting the typical plasmon band in two signals. The transverse plasmon band is typically centred at 520 nm for Au nanoparticles and at 420 nm for Ag nanoparticles, while the longitudinal plasmon band position depends on the ratio between the length and diameter (aspect ratio) of the nanoparticle. Therefore, a fine-tuning of the aspect ratio of metal NRs allows us to shift the position of the longitudinal plasmon band across the whole visible-NIR range (Figure 5) [2,49,53]. Furthermore, the increase in the aspect ratio results in a non-linear increase of the full width at half maximum (FWHM) of longer wavelength absorption peak [54].

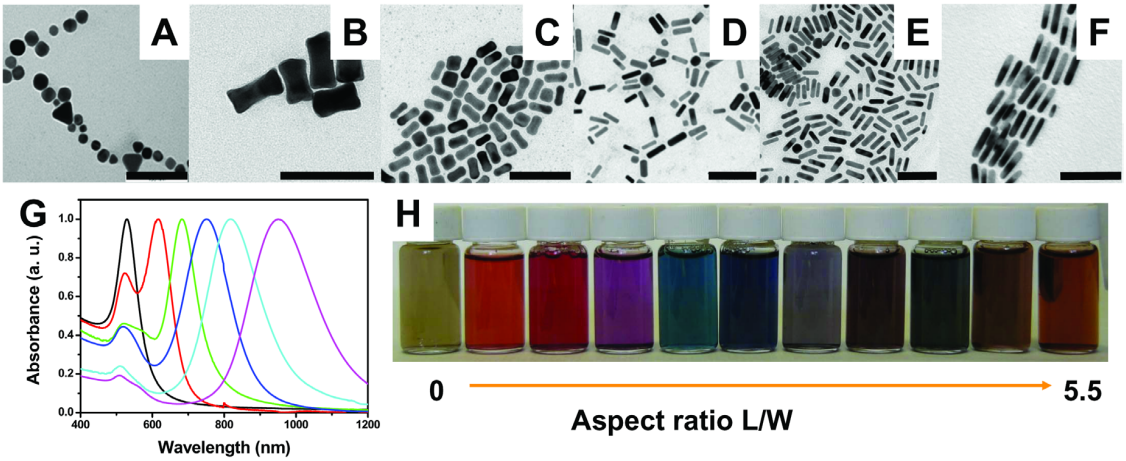

Figure 5. Shape dependence of surface plasmon resonance of Au NRs at increasing aspect ratios. (**A**–**F**) TEM Images of Au nanoparticles with aspect ratio ranging from 1 (**A**) to 5.5 (**F**) (**G**) Absorbance spectra of samples reported in (**A**–**F**): black line sample A, red sample B, green sample C, blue sample D, cyan sample E, purple sample F; (**H**) Visual appearance of Au nanoparticles water solution as a function of aspect ratio. Reprinted with permission from [55]. Copyright 2015, Pan Stanford Publishing.

Several papers demonstrate a great improvement in visible-light-driven photocatalysis upon deposition of Ag and Au nanoparticles onto TiO_2 nanostructures [2,18,20,56–58]. However, the mechanism behind such an enhancement is still under debate. Three main hypotheses have been proposed so far:

- plasmon resonance effect: the direct injection of the electron excited from metal nanoparticles under visible radiation into the conduction band of the semiconductor is expected to occur [59,60];

- near-field effect: the plasmon resonance induces an electric field that causes a plasmon resonance energy transfer (PRET) from metal to TiO_2. Such a PRET phenomenon is thought to enhance the electric field in a well-defined location resulting in a rapid formation of e^-/h^+ pairs [61–64];
- far-field effect: an efficient scattering can be mediated by surface plasmon resonance, which increases the optical path of photons in TiO_2 that improve the excitation of e^-/h^+ pairs [65].

Moreover, noble metal nanoparticles can store photogenerated electrons, thus promoting charge separation in semiconductor–metal composite systems [66,67]. Several other factors may also affect photocatalytic efficiency, e.g., the surface properties, the particle size of the catalysts their morphology, and the composition and organization of the metal and TiO_2 [68]. Therefore, great efforts have been devoted to the synthesis of well-controlled and highly efficient plasmonic metal–TiO_2 nanostructures [16,18,37]. Various synthetic approaches have been reported for the synthesis of TiO_2 and metal nanoparticle hybrid heterostructures. These include impregnation [69], UV irradiation [66], electrodeposition [70], sonochemistry [71], and hydrothermal [72], sol-gel [73], and flame-spray synthesis [74]. Although these methods have been demonstrated to be quite effective, getting fine control over particle size, size distribution and composition in the final materials still remains challenging [75]. Interestingly, noble metal loading of 1% or lower is generally regarded as optimal for a significant increase in the photocatalytic activity [58,76,77].

2.2.1. Chemical Reduction of Metals at the TiO_2 Surface

Chemical reduction of metals at the TiO_2 surface is one of the simplest and most widely used methods for the preparation of plasmonic metal–TiO_2 nano-heterostructures. The general protocol involves the adsorption of metal precursors on the TiO_2 nanoparticle surface, followed by chemical reduction. Several reducing agents have been used to prepare Au or Ag nanoparticle-based TiO_2 hybrid nanocrystals [16], namely: sodium citrate (Turkevich method) [78], sodium borohydride (Brust method) [79] and other organic reagents [80]. For instance, water-dispersible anatase TiO_2 colloidal spheres of ~220 nm in diameter have been exploited as templates to nucleate and grow Au nanoparticles on their surface. Such an approach employs $AuCl^{4-}{}_{(aq)}$ as the Au precursor, ascorbic acid as the reducing agent, and PVP as the stabilizer. It is worth noting that Au nanoparticle deposition does not require any chemical modification at the TiO_2 surface. Furthermore, the Au nanoparticle size could be tuned by performing sequential $AuCl^{4-}{}_{(aq)}$ reduction steps [75]. For instance, 5.7 nm Au nanoparticles have been deposited on the surface of TiO_2 P25 Aeroxide from Evonik (formerly known as TiO_2 P25 Degussa) by in situ chemical reduction in water. Trisodium citrate has been utilized to control and stabilize the growth of Au nanoparticles and to attain a nearly monodisperse size distribution, whereas $NaBH_4$ has been selected as the reducing agent [68]. Au nanoparticles can be grown onto semiconductor structures by a deposition–precipitation procedure, followed by calcination, as reported by Silva and co-workers [81]. Indeed, to achieve the deposition of Au nanoparticles on P25 TiO_2 $HAuCl_4$ has been reduced at 343 K and pH 9, followed by calcination at 673 K in air for 4 h. However, these two methods show poor control over the morphology of noble metal nanocrystals and are not able to avoid aggregation of metal nanoparticles, which may further limit their application [82].

2.2.2. Photochemical Reduction of Metals at the TiO_2 Surface

Metal ions could be directly reduced at the semiconductor surfaces by using the electrons and holes generated by the irradiation of TiO_2 with UV light. Various hybrid nanocrystals such as TiO_2–Ag [83] and TiO_2–Au have been prepared by a photo-reduction method [84]. For instance, this approach has been applied to grow Ag or Au nanoparticles onto TiO_2 NRs [85,86] or on TiO_2 supported on glass fibres [87], thus generating heterostructures. Photodeposition of Au on sulphated TiO_2 (S–TiO_2) has been realised by illuminating gold salt under an inert atmosphere (N_2) with a lamp having a sun-like radiation spectrum and a main emission line in the UVA range at 365 nm, in a suspension of S–TiO_2 in distilled water containing isopropanol, which acts as a sacrificial donor [88].

Recently, a visible active multifunctional nano-heterostructure, composed of a TiO_2 NR, and Fe_3O_4 and Ag nanoparticles (TiO_2NRs/Fe_3O_4/Ag), has been prepared by our group. The obtained photocatalyst merges distinct multiple functions in one nanostructure: (i) the high photocatalytic efficiency of rod-shaped TiO_2 nanocrystals; (ii) the magnetic properties of Fe_3O_4, able to promote, in principle the magnetic recovery of the photocatalyst; and (iii) Ag nanoparticles able to extend the photocatalytic activity of the system to the visible region. The synthesis of the ternary heterostructure TiO_2NRs/Fe_3O_4/Ag has been carried out in a three-step procedure. The first and second steps involve the synthesis of TiO_2 NRs and TiO_2/Fe_3O_4 heterostructures, respectively, according to the reported procedures [89]. Finally, TiO_2NRs/Fe_3O_4/Ag heterostructures have been prepared by photochemical reduction of Ag^+ at the TiO_2NRs/Fe_3O_4 surface under UV irradiation and an inert atmosphere [2].

2.2.3. Growth of a TiO_2 Shell at a Plasmonic Nanoparticle Surface

Coating plasmonic metal nanoparticles with TiO_2 is another promising method [90]. Indeed, a TiO_2 shell can prevent the metal nanoparticles from aggregation, while versatile nanostructures can be obtained by coating different shapes of metal nanoparticles [82]; Ag@TiO_2 nanostructures have been realized by the hydrolysis of titanium precursor on Ag core [56,91]. Similarly, Au nanoparticles have been coated with a TiO_2 shell by the hydrolysis of the titanium precursor [92,93]. Gold/Silver/Titania tri-layer core/shell/shell hybrid nanocrystals have been reported, demonstrating photocatalytic activity in the visible range [94]. Also, rod-like anisotropic Au nanoparticles have been coated with a TiO_2 shell, demonstrating the capability to enlarge the photoactivity of TiO_2 to visible light, owing to the presence of a longitudinal plasmon band [95,96].

Templates have been used to prepare sandwich-type nanostructures, like those prepared by Zhang et al., composed of SiO_2/Au/TiO_2 by a sol-gel process. SiO_2 particles of 400 nm in diameter have been synthesised and functionalised with (3-aminopropyl)triethoxylsilane (APTES). In a second step, Au nanoparticles have been bound at the silica surface; subsequently, an amorphous TiO_2 shell has been grown on SiO_2/Au hybrid particles [97].

Recently, a TiO_2 shell with a thickness of about 4.5 nm has been grown onto a pre-synthetized Au NRs and Au/Ag core-shell NRs with aspect ratio of 2.3 by letting react titanium-(triethanolaminato) isopropoxide (TTEAIP) in isopropanol (80%) for 24 h under continuous stirring [98]. The UV-Vis extinction spectrum of the Au/TiO_2 core-shell nanoparticles dispersed in water (Figure 6c) displayed a longitudinal surface plasmon resonance (SPR) band at 670 nm. Figure 5D,E show the TEM images of the prepared Au/Ag core-shell NRs and Au/Ag/TiO_2 hybrid nanoparticles. The uniform TiO_2 shell onto the Au/Ag core of the hybrid nanoparticles can be observed in the TEM images (Figure 6e). The UV-Vis extinction spectrum of the Au/Ag/TiO_2 core-shell nanoparticles in water (Figure 6f) is characterised by a longitudinal SPR band centred at 670 nm.

2.2.4. Other Approaches

Recently, Au nanoparticles have been supported on TiO_2–C_3N_4 for CO oxidation under visible light irradiation. Firstly, heterostructured TiO_2–C_3N_4 microspheres have been prepared by using a hydrothermal method starting from titanium glycolate as a precursor and graphitic C_3N_4. Then, the TiO_2–C_3N_4 microspheres have been decorated with Au nanoparticles by letting $HAuCl_4$ react at alkaline pH (pH = 10) in the presence of Na_2CO_3. After washing and drying overnight, the powder has been calcinated at 350 °C for 2 h to obtain the catalysts [99].

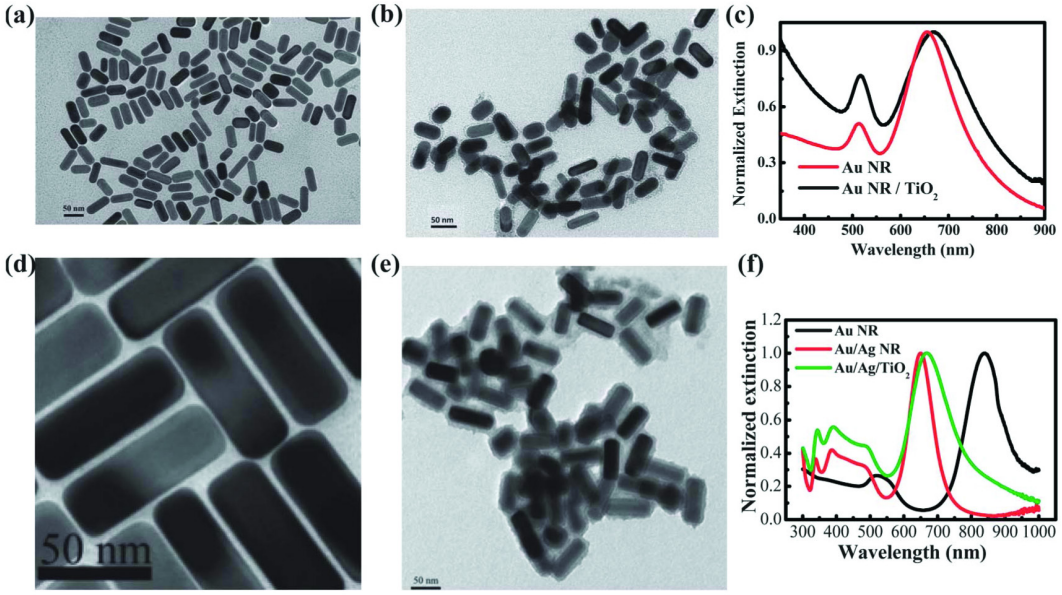

Figure 6. TEM images of Au NRs (**a**); Au/TiO_2 core-shell nanoparticles (**b**); Au/Ag NRs (**d**) and Au/Ag/TiO_2 core-shell nanoparticles (**e**). Their UV-Vis extinction spectra are shown in (**c**,**f**). The extinction spectrum of Au NRs used for preparation of Au/Ag NRs in reported in (**f**). Reprinted with permission from [67]. Copyright 2013, Royal Society of Chemistry.

Au–CuS–TiO_2 nanobelts (NBs) have also been successfully synthesised using a three-step approach and then applied for environmental remediation. Indeed, TiO_2 NBs have been prepared by electrochemical anodic oxidation. In the second step, CuS nanoparticles have been deposited on TiO_2 by the SILAR method (Successive ionic layer adsorption and reaction); finally, Au nanoparticles, have been electrodeposited on CuS/TiO_2 heterostuctures. Photoelectrochemical and photoluminescence investigation have demonstrated that the Au–CuS–TiO_2 NBs nanostructure hampers the recombination of photogenerated e^-/h^+ pairs due to the efficient interfacial charge transfer. The ternary Au–CuS–TiO_2 NBs have demonstrated improved photocatalytic activity in removing the antibiotic oxytetracycline (OTC) in an aqueous solution under simulated solar irradiation [100].

A one-pot solvothermal approach has been proposed for the fabrication of an Ag/Reduced Graphene Oxide/TiO_2 heterostructure, where Ag nanoparticles are generated from the reduction of $AgNO_3$ by dimethylacetamide [101].

Photocatalytic noble metallic and bimetallic hybrid nanocomposites (Ag/TiO_2/CNT) have been synthesised using a commercial source of multi-walled carbon nanotubes MWCNTs via a modified dry-mix metal–organic chemical vapour deposition method (MOCVD). In the first step, TiO_2 nanoparticles have been grown at the MWCNTs' surface by MOCVD. To deposit Ag onto the TiO_2/CNTs, a defined amount of Ag acetylacetonate (97.5% purity) has been mixed with the nanocomposite structures and subjected to the MOCVD process [102].

2.3. TiO_2-Based Hybrid Nanocrystals, Including Magnetic Nanoparticles

The technological challenges related to the release of nanopowders into the environment need to be addressed by developing nanomaterials that are easy to recover and reuse. For this reason, a great deal of work has been devoted to enriching the properties of TiO_2 by rationally designed, magnetically recoverable hybrid nanocrystals able to perform photocatalytic reactions under visible light. Such heterostructures merge into one nano-system a photocatalytic moiety, namely TiO_2 nanocrystals, with a second component able to show magnetic properties and, in most cases, with a third unit able to extend the optical response of the system in the range of visible light. For TiO_2-based magnetic hybrid nanocrystals, the typical configuration involves a magnetic core of Fe_3O_4 and a

photoactive shell of TiO_2. Furthermore, in order to achieve a visible-light-active photocatalyst, the outer layer of TiO_2 is often functionalised with an additional component, able to absorb visible light as noble metal nanoparticles, carbon-based nanomaterials or low band gap semiconductors that have been described in detail in other sections of the present review. The core-shell morphology is often selected in order to design magnetically recoverable photocatalysts because it has the advantage of limiting the Fe_3O_4 dissolution and, at the same time, maximising the interaction between visible light and the photoactive component. Recently, Fe_3O_4@TiO_2/Ag hybrid nanocrystals have been prepared by a multistep procedure that starts with the formation of citrate-capped Fe_3O_4 nanoparticles, stable in polar solvents, thus facilitating the uniform growth of the TiO_2 shell. The formation of a mesoporous shell of TiO_2 occurs by a hydrothermal approach that, employing temperatures under 160 °C, preserves the magnetic properties of the Fe_3O_4 core and at the same time induces the generation of an anatase phase. The final step consists in the decoration of the heterostructure with Ag nanoparticles, resulting in a good photochemical response under visible light [103]. Tang et al. have prepared a visible-light-active photocatalyst with a supplementary functionality. The proposed heterostructure comprises a core of Fe_3O_4 separated from TiO_2 by a SiO_2 intralayer. The obtained Fe_3O_4@SiO_2@TiO_2 heterostructures have been further functionalised with reduced graphene oxide (RGO), resulting in the Fe_3O_4@SiO_2@TiO_2-RGO. In such an elaborate system, each component plays a specific role: the TiO_2 is the main photocatalyst, the RGO provides visible light photocatalytic activity and improves the e^-/h^+ separation, while the SiO_2 intralayer avoids the photodissolution of Fe_3O_4, which finally ensures the magnetic recovery of the resulting powder. The preparation of such heterostructures requires the combination of several steps and synthetic techniques in order to provide a close interaction among the different components involved. Pre-synthesised Fe_3O_4 nanoparticles have been first silanised and coated with a layer of TiO_2 a sol-gel procedure, which makes use of tetra-*n*-butyl titanate as a TiO_2 precursor. Subsequently, the RGO has been connected to the heterostructure by an aminopropyltrimethoxysilane mediated assembling process [104].

In a similar core-shell heterostructure, the visible light photocatalytic activity has been accomplished by growing an Ag_3PO_4 shell onto a Fe_3O_4@TiO_2 core-shell system. The magnetic photocatalyst has been effective both in the photodegradation of a model dye, as well as in bacteria inactivation under visible light. Interestingly, the magnetic properties of the Fe_3O_4 core have also been exploited during the synthetic procedure to separate heterostructures from the reaction medium. In this case, the TiO_2 has nucleated onto Fe_3O_4 nanoparticles thanks to the hydrolysis of $Ti(SO_4)_2$ that promotes the formation of a layer of anatase TiO_2 wrapped around the Fe_3O_4. Finally, the deposition of Ag_3PO_4 occurred by a precipitation method, giving rise to Ag_3PO_4 nanoparticles at the surface of Fe_3O_4@TiO_2 [105].

An alternative geometry of TiO_2/Fe_3O_4-based heterostructures has been achieved by promoting the direct growth of Fe_3O_4 on nanosheets of TiO_2. TiO_2 nanosheets, indeed, are expected to provide an improved photocatalytic activity due to a faster interfacial electron transfer and an increased exposure of the {010} facet, which implies a higher number of surface OH groups. The formation of anatase and a rutile TiO_2 nanosheet has been promoted by the hydrolysis of titanium (IV) tetraisopropoxide in the presence of Pluronic P123, while spherical Fe_3O_4 nanoparticles have been synthesised in the presence of TiO_2 nanosheets, by $FeCl_3$ as a precursor, thus obtaining the final TiO_2/Fe_3O_4 heterostructure [106].

Besides Fe_3O_4, TiO_2 nanocrystals can also be bound to other magnetic nanoparticles as ferrites. $CoFe_2O_4$ have been coupled with TiO_2 NRs and a polyaniline (PANI) to achieve a flowerlike architecture of micrometric dimensions with photoactivity under visible light. $CoFe_2O_4$ spheres, 20 nm in size, have been synthesised in the presence of sodium bis-(2-ethylhexyl) sulfosuccinate as the surfactant that forms inverse micelles in water in an oil microemulsion. Such a system is known to work as a nanoreactor, promoting the formation of nanospheres. Subsequently, the formation of TiO_2 has been achieved by means of a hydrothermal method in the presence of $CoFe_2O_4$. Finally, PANI has been integrated in the obtained heterostructure by an in situ polymerization method by using aniline as a monomer. The resulting heterostructures have shown a hierarchical, flower-like geometry,

consisting of TiO_2 NRs, assembled in a thorn-like arrangement, covered by the $CoFe_2O_4$ nanospheres and functionalised with PANI as a co-catalyst [107].

2.4. Heterostructures Containing C-Based Materials

New allotropes of carbon such as carbon nanotubes (CNTs), graphene (G), carbon dots (C-dots) and graphitic carbon nitride (C_3N_4) have emerged in the last few years as effective and fascinating C-based nanomaterials to improve the photocatalytic activity of TiO_2. Besides their high surface area, which implies an improved ability to absorb organic pollutants, they share the property of decreasing the e^-/h^+ recombination rate, because C-based nanomaterials can effectively scavenge photoexcited electrons from the conduction band of TiO_2. Furthermore, when they are combined with TiO_2, they can provide visible light photocatalytic activity for two main reasons, according to the specific heterostructures. When C-dots and C_3N_4 are combined with TiO_2, forming heterostructures, they can act as photosensitizers, both being narrow band-gap semiconductors. CNTs-TiO_2-based heterostructures show visible light photocatalytic activity according to the nature of CNTs (metallic CNTs, semiconducting CNTs, Multi-Walled CNTs or Single-Walled CNTs). Finally, the visible light photocatalytic activity of G-TiO_2 heterostructures is proposed to arise from a doping effect that is due to the formation of Ti–O–C bonds [108]. The synthetic techniques to prepare CNTs-TiO_2, G-TiO_2, C-dots-TiO_2 and C_3N_4-TiO_2 heterostructures aim to obtain close contact between TiO_2 and the carbon-based material to form a heterojunction able to maximise the interplay with TiO_2. An additional goal of the synthesis procedure is to obtain a good dispersion of anatase TiO_2 nanocrystal on the C-based support; however, only a few works report strict control over the size and shape of TiO_2 nanocrystals in C-based heterostructures. The present section will describe selected procedures recently reported in the literature for the preparation of carbon-based TiO_2 heterostructures that have been demonstrated to be photoactive under visible light [108,109].

2.4.1. CNTs-TiO_2-Based Heterostructures

CNTs-TiO_2-based heterostructures are promising visible-light-active photocatalysts. In general, the preparation methods of CNTs-TiO_2 heterostructures aim to obtain a core-shell system where TiO_2 nanocrystal growth occurs directly on the CNTs' surface, thus resulting in a uniform coating. Such a goal is often accomplished by functionalising the surface of CNTs with carboxylic groups that can anchor the precursors of TiO_2 nanocrystals. Indeed, in a recent report, multi-walled CNTs (MWCNTs) have been functionalised with COOH groups that favour the growth of TiO_2 nanocrystals, which takes place by means of the hydrolysis of $Ti(OBu)_4$ in ethanol, followed by calcination. The procedure allows us to obtain a uniform dispersion of TiO_2 nanoparticles, limiting TiO_2 aggregation and favouring the growth along the {101} direction. The obtained TiO_2/MWCNTs heterostructures have shown an absorption edge at 400 nm and photoactivity under visible light [110]. Alternatively, TiO_2 nanocrystals can be grown on SWCNTs (single walled carbon nanotubes) without the need for COOH moieties, just using a treatment with strong oxidizing acids—which, however, negatively affects the conductivity of CNTs [111]. SWCNTs dispersed in oleic acid have been exploited as a platform to obtain the direct growth of spherical (TiO_2 dots) or rod-shaped TiO_2 nanoparticles (TiO_2 NRs). The synthetic scheme involves the dispersion of SWCNTs in oleic acid and the subsequent injection of the Ti(*i*PrO)$_4$ as a TiO_2 nanocrystal precursor. When the introduction of Ti(*i*PrO)$_4$ occurs in the presence of an excess of water, TiO_2 NRs have been observed on the SWCNTs' surface; conversely, when a reduced amount of water is formed in situ, the TiO_2 nanosphere is grown directly on the SWCNT surface. Therefore, the amount of water in the reaction mixture drives the growth of rod-shaped or spherical nanocrystals on the SWCNT surface and, accordingly, SWCNTs/TiO_2 NRs or SWCNTs/TiO_2 dot heterostructures can be obtained. It is worth noting that the shape of TiO_2 nanoparticles in this case affects the photocatalytic activity of the heterostructure. Indeed, only SWCNTs/TiO_2 NRs have demonstrated improved photocatalytic activity under visible light. The authors explained that this results from invoking a doping-like effect,

induced by the Ti–O–C bonds that are supposed to be more abundant in the case of SWCNTs/TiO_2 NRs, due to the higher contact between SWCNT and TiO_2 nanocrystals [17].

2.4.2. Graphene-TiO_2-Based Heterostructures

Graphene (G) has been widely exploited to improve the photocatalytic activity of TiO_2 nanocrystals. A visible-light-active TiO_2-G-based photocatalyst has been achieved by Ismail and coworkers, who have synthesised TiO_2-G-based heterostructures by carrying out the thermal treatment in oxidizing, inert or reducing atmospheres. Their work demonstrated that when an oxidizing atmosphere is used, along with the calcination step, graphene–oxide TiO_2 heterostructures (TiO_2-GO) are obtained and it is possible to control their morphology by tuning the amount of TiO_2 precursor, namely Ti(*i*PrO)$_4$. In particular, a low amount of Ti(*i*PrO)$_4$ gives rise to sheet-like structures with high thickness, smooth surface and wrinkled edges; conversely, a high amount of Ti(*i*PrO)$_4$ produces uniform and high-density TiO_2 particles on the entire GO surface [112].

In order to finely tune the morphology of TiO_2 nanocrystals on the reduced graphene oxide surface (RGO), a possible strategy consists of the use of SiO_2 nanospheres as a sacrificial template. The procedure started with the synthesis of SiO_2 nanospheres and the subsequent fabrication of a TiO_2 layer on the SiO_2 surface. The obtained nanocomposite reacts with GO by a chemical bonding reaction. Such a process consists of a reaction between the as-prepared TiO_2–SiO_2 nanocomposite and the GO. In particular, a water suspension of GO was dispersed in an ultrasonic bath; after that, TiO_2–SiO_2 was added to the dispersion and the system was stirred for 12 h in order to allow the encapsulation process. This step promoted the formation of Ti–C bonds according to the X-ray photoelectron spectroscopy (XPS) characterisation. After the elimination of the SiO_2 template with NaOH, the sample was calcinated at 180 °C in order to promote the formation of the anatase phase. The subsequent hydrothermal reactions carried out in an autoclave and a microwave allowed us to transform GO into RGO, thus finally obtaining a heterostructure of RGO and TiO_2 hollow nanospheres [113].

G-TiO_2-based heterostructures have also been achieved with anisotropic TiO_2 nanocrystals. Such a heterostructure consists of graphene sheets functionalised with TiO_2 NRs in a sandwich-like arrangement. In this work, TiO_2 NRs have been grown on the G surface via a "seed-directed" hydrothermal route. According this procedure, Ti(OBu)$_4$ has been dispersed in an ultrasonic bath in the presence of G. The subsequent thermal treatment resulted in the formation of TiO_2 seeds on the G surface. Then, the growth of TiO_2 NRs was achieved by adding an extra amount of TiO_2 precursor and repeating the hydrothermal procedure [114].

2.4.3. Other C-Based TiO_2 Heterostructures

C-dot, namely carbogenic carbon dots, are new carbon-based nanomaterials showing outstanding properties including high chemical stability, low toxicity and biocompatibility; in addition, they can be easily functionalised. Moreover, they display size-dependent visible light absorption and high photoluminescence properties. Accordingly, C-dots have a great potential for the functionalisation of TiO_2 with the aim of developing visible-light-active heterostructures. Liu and co-workers have synthesised a hierarchic TiO_2 heterostructure in the presence of pre-synthesised C-dot. Such heterostructures have been designed in order to improve the recoverability of the photocatalyst and obtain a visible-light-active photocatalyst. In particular, the heterostructure consists of TiO_2 NRs assembled in a microsphere of micrometric size. Subsequently, C-dots are anchored on TiO_2 microspheres uniformly covering the surface. The obtained heterostructures have demonstrated improved photocatalytic activity in the visible range in the degradation of rhodamine B in water [115].

Hybrid nanocrystals that combine C-dot and TiO_2 nanoparticles can also be obtained by directly synthesising in situ the two components in a one-step process (Figure 7). Such a goal has been achieved by realizing the hydrothermal growth of C-dot and TiO_2 directly in situ on graphene oxide as a supporting co-catalyst, exploiting glucose and $TiCl_4$ as precursors. The authors have remarked that the presence of glucose also affected the growth of TiO_2 nanocrystals. Because of the abundance of

–OH groups, glucose molecules can surround TiO_2 nanocrystals, controlling their increase in size and limiting their aggregation [116].

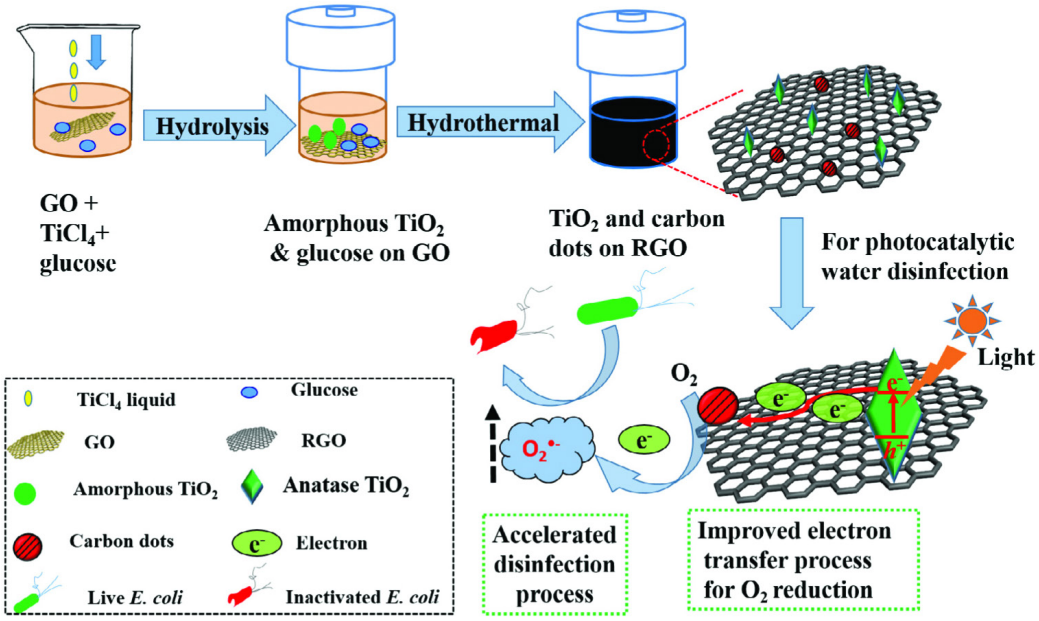

Figure 7. Illustration of the synthesis of a C-dot-TiO_2-reduced graphene oxide nanocomposite and its application for photocatalytic water disinfection [116]. Copyright 2017, Elsevier.

C_3N_4 has been successfully exploited in the literature in order to convey visible light photocatalytic activity to TiO_2 nanocrystals. In particular, graphitic C_3N_4 (g-C_3N_4) enhances the photocatalytic activity of TiO_2 because it displays a band gap of 2.69 eV (i.e., in the visible range), high thermal and chemical stability, and, like all C-based nanomaterials herein examined, can decrease the e^-/h^+ recombination events. The growth of TiO_2 nanocrystals has been reported to occur directly on pre-synthesised g-C_3N_4 in the presence of arginine. The role played by arginine is to functionalise the surface of g-C_3N_4 by electrostatic interaction of H-bonds. When the negatively charged TiO_2 precursor (Titanium (IV) bis-(ammonium lactato) dihydroxide Ti-BALDH) is added to the reaction mixture, an H bond is formed. In particular, such an H bond involves the H atom of Ti–OH of the Ti-BALDH and the N atom of the C=NH group of arginine. The authors proposed that, thanks to this H-bond, the O atom of the Ti–OH group attacks a Ti atom of an adjacent Ti-BALDH molecule, according to a nucleofilic attack mechanism, thus resulting in a polycondensation reaction. The obtained heterostructure is characterised by g-C_3N_4 nanosheets, uniformly covered by TiO_2 nanoparticles 10 nm in size. The heterostructure has a specific surface are of 109 m^2/g and displays a notable absorption in the visible light region [117].

3. Applications

3.1. Water Remediation

In the present section we give an overview of recently proposed TiO_2-based heterostructures specifically designed for water purification by visible-light-driven photocatalysis. The increase in the amount and diversity of pollutants in ground and surface water has been caused by rapidly broadening industrialization and population growth. The European Directive 2000/60/CE has highlighted the need to adopt measures against water pollution in order to achieve a progressive reduction of pollutants [118]. Among the main causes of such increasing pollution is waste disposal into the water bodies from industry, which also induces the growth of micro-organisms in water [119]. Moreover, pollutants may also enter the water indirectly due to the use of plant health products in

agriculture, as fertilizers and biocides. Indeed, one the major threats to water quality is chemical pollution from heavy metals, solvents, dyes, pesticides, antibiotics, etc.

In recent years, different alternatives for water cleaning such as adsorption or coagulation methods aimed just at concentrating pollutants by transferring them to other phases, without their complete elimination [120]. Alternative methods such as sedimentation, filtration, chemical and membrane technologies involve high operating costs and could generate toxic secondary pollutants in the ecosystem [121]. Conventional methods such as chlorination are widely used disinfection processes; however, chlorine can react with organic matter and other precursors to form regulated and emerging disinfection byproducts, which can be associated with cancer or another human pathologies [122]. These concerns have rapidly increased the interest of the scientific community in the field of "Advanced Oxidation Processes (AOPs)" as possible innovative alternatives to conventional disinfection processes. Water treatment based on photocatalysis provides an important choice with respect to the other advanced oxidation technologies such as UV-H_2O_2 and UV-O_3. In particular, solar-based photocatalytic AOPs is one of the most promising, safe, low-cost and effective technologies for polluted water treatment, and has been applied to a wide range of environmental pollution situations [123]. Among AOPs, TiO_2-based photocatalysis has recently emerged as an interesting water disinfection option for solar applications [122], due to its high oxidative efficiency, photochemical stability, nontoxicity and low cost. However, the high recombination ratio of photoinduced e^-/h^+ pairs and the poor response to visible light have hindered the application of TiO_2 in photocatalysis. The current challenge is to investigate new photocatalysts based on TiO_2 nanoparticles suitably modified to shift the absorption edge of TiO_2 toward the visible region. Visible-light-active photocatalysts based on TiO_2 heterostructures have been exploited in the treatment of inorganic, organic, and biological contaminated water [124].

A promising approach to enhance photocatalysis in the visible is to deposit a noble metal (Au, Ag) on the semiconductor nanoparticle surface, resulting in a semiconductor–noble metal heterostructure. This results in (1) surface plasmon resonance-induced photosensitization, which can be used to harvest visible light, and (2) the formation of a Schottky barrier at the noble metal–semiconductor interface, leading to a decrease in e^-/h^+ recombination. For instance, the photocatalytic activity of Au NR/TiO_2 and Au/Ag NR/TiO_2 core-shell nanoparticles has been evaluated by the degradation of methylene blue, driven by visible light irradiation. It has been demonstrated that Au or Au/Ag NRs enhance the photocatalytic activity of TiO_2. A reasonable mechanism beyond the enhanced photocatalytic dye degradation is reported in Figure 8 [67].

In this case, the bimetallic Au/Ag core-shell NRs have shown significantly enhanced visible light photocatalytic efficiency due to their effective light absorption in the visible range. In addition, it has been shown that the position of longitudinal SPR of Au/Ag core-shell NRs could be tuned across the entire visible spectral range as a function of the Ag shell thickness. However, the high cost of gold limits the applications of Au/TiO_2. Recently, a visible-light-active, silver-modified titania catalyst has been reported by Kowalska et al., for application in the decomposition of methanol, acetic acid, 2-propanol and *Escherichia coli*. In particular, antibacterial properties have been enhanced by visible light irradiation and modification with Ag nanoparticles. The increase of these properties under visible light has indicated that the intrinsic properties of Ag in the dark and the plasmonic properties of Ag/TiO_2 have been responsible for overall bacteria killing [125].

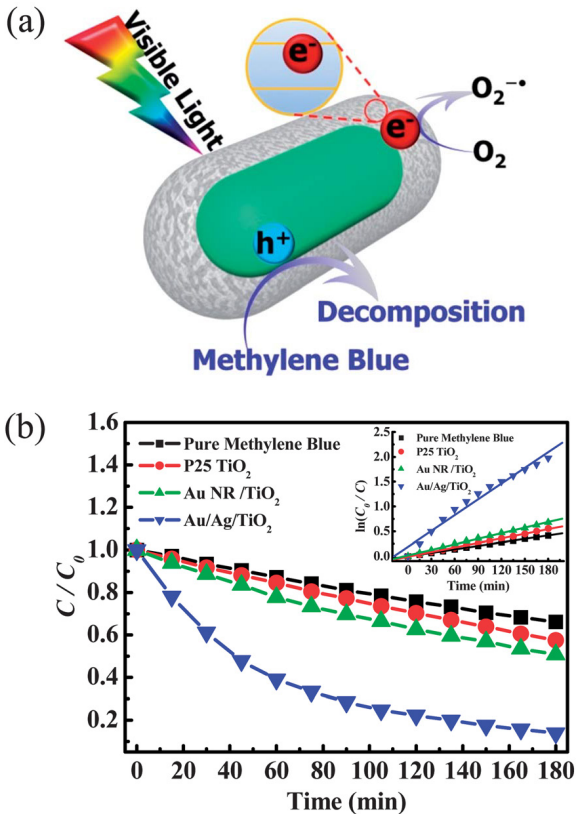

Figure 8. (**a**) Schematic representation for the mechanism of photocatalytic degradation of dyes upon visible light excitation of Au/TiO_2 NRs (**b**) Time monitoring of photocatalytic degradation of methylene blue (MB) under visible light irradiation in the absence and presence of photocatalysts (P25-TiO_2, $Au/Ag/TiO_2$ core-shell nanoparticles). Reprinted with permission from [67]. Copyright 2013, Royal Society of Chemistry.

Nowadays, a reliable use of nanomaterials for photocatalytic degradation of pollutants, especially for water and wastewater purification, poses important concerns about the safe recovery and reuse of nanoparticles. Deposition of photocatalysts on substrates in the form of thin films could significantly simplify the separation procedure. As a possible solution, wood substrates (or natural organic polymer materials) have been used as profitable host materials of inorganic particles because the excellent electrical, magnetic and optical properties of inorganic materials can be preserved in the polymer matrix. In a recent study reported by Gao et al., Ag/TiO_2-coated wood has been reported as a portable photocatalyst for green applications in the degradation of phenol, which could be easily removed from polluted water after use. Specifically, the wood decorated with Ag/TiO_2 composite film presented multiple properties, such as super-hydrophobicity, antibacterial actions against both Gram-negative (*Escherichia coli*) and Gram-positive (*Staphylococcus aureus*) bacteria, and photodegradation of phenol under visible light [126].

Moreover, recently, magnetic TiO_2 nanocomposites with core-shell structure have also gained increasing attention, as they can integrate the advantages of magnetic recovery and superior photocatalysis performance. A possible strategy is based on visible-light-active, multifunctional nanostructures, which show great promise as efficient and recyclable photocatalysts for environmental remediation. Petronella et al. have evaluated the efficiency of $TiO_2NRs/Fe_xO_y/Ag$ in the photocatalytic degradation of the antibiotic nalidixic acid (NA) under visible light. The experimental results demonstrated that the $TiO_2NRs/Fe_xO_y/Ag$ nanostructure, with Ag nanoparticles of 12 nm in size, was 1.9 times faster than the commercial TiO_2 P25 and 1.5 times faster than the TiO_2NRs. Such an enhancement has been accounted for by the presence of Ag nanoparticles that enhance visible light

photoactivity due to their peculiar plasmonic properties (Figure 9) [20]. These materials can be easily removed and recycled by applying an external magnetic field.

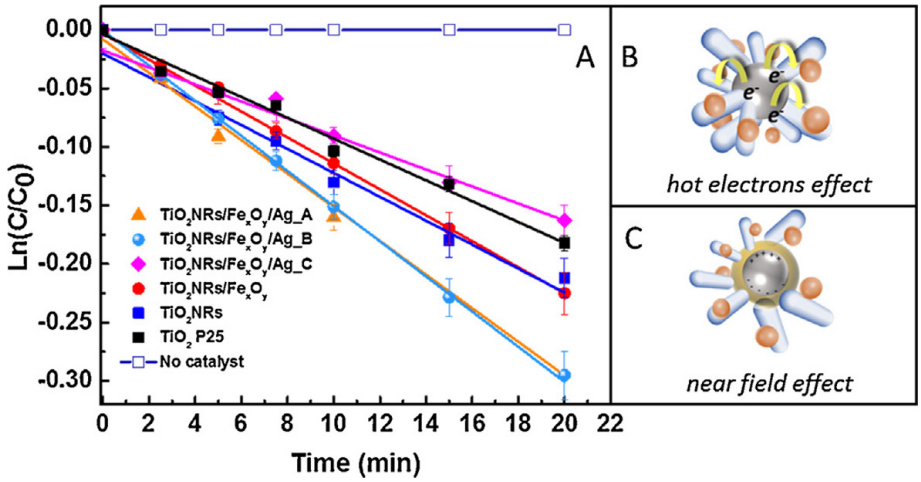

Figure 9. (**A**) Nalidixic acid degradation rates in the presence of TiO_2NRs/Fe_xO_y/Ag_A, TiO_2NRs/Fe_xO_y/Ag_B and TiO_2NRs/Fe_xO_y/Ag_C, TiO_2NRs/Fe_xO_y, TiO_2NRs and TiO_2P25. Experiments carried out at pH 2.5 under visible light irradiation. Nalidixic acid concentration evaluated by monitoring the absorbance intensity at 316 nm (pH 2.5). (**B** and **C**) Scheme of possible photoactivation mechanism of the TiO_2NRs/Fe_xO_y/Ag under visible light: hot electrons effect (**B**) and near field effect (**C**) Reprinted with permission from [20]. Copyright 2016, Elsevier.

Furthermore, Wang et al. have synthesised TiO_2NRs/Fe_xO_y/Ag core-shell nanostructures exhibiting remarkably efficient enhancement of photocatalytic degradation of Rhodamine B, even under visible light and solar light irradiation [103].

In a recent review, it has been reported that aqueous pollutants such as methylene blue, benzene derivatives and carbamazepine have been efficiently photodegraded by CNT/TiO_2 nanostructured composites [127]. In this case, the bond of carbon–oxygen–titanium can expand the light absorption towards longer wavelengths according to a C-doping-like mechanism and therefore potentially lead to the enhancement of photocatalytic activity under visible light. In addition, CNTs could act as micrometric supports to be dispersed in contaminated water and recovered by decantation or filtration. As an example, SWCNT/TiO_2 NRs heterostructures have been successfully employed for the degradation of a mixture of 22 selected organic pollutants in real secondary wastewater effluent under simulated solar light. This photocatalyst presents high efficiency, can be easily recovered from the aqueous solution by mild centrifugation or filtration and, consequently, could be reused for subsequent batches of photocatalytic treatment [19].

Similarly, two semiconductors possessing different CB and VB energy levels can also be effectively coupled to enhance photocatalytic properties. Such an enhancement is explained as a result of vectorial transfer of photogenerated electrons and holes from one semiconductor to another, thus inhibiting the recombination of e^-/h^+ pairs, e.g., WO_3/TiO_2 [35], In_2O_3/TiO_2 [34], Bi_2O_3/TiO_2 [128], RGO/TiO_2 [129]. In particular, Yang et al. have investigated the effect of the coupled Bi_2O_3/TiO_2 photocatalysts on the photocatalytic reduction of Cr(VI) with the synergistic effect of photodegradation bisphenol A (BPA) in an aqueous solution under visible-light irradiation. These photocatalysts, at different Bi_2O_3 dosages, have been fabricated by sol-gel and hydrothermal process. For example, 2.0% Bi_2O_3/TiO_2 exhibited the highest photocatalytic activity of visible-light-induced reduction of Cr(VI). Upon irradiation by visible light, photo-electrons, generated by exciting Bi_2O_3, promoted the reduction of Cr(VI) to Cr(III). The addition of BPA increased the photocatalytic reduction of Cr(VI) and the presence of Cr(VI) significantly promoted the degradation of BPA (Figure 10) [128].

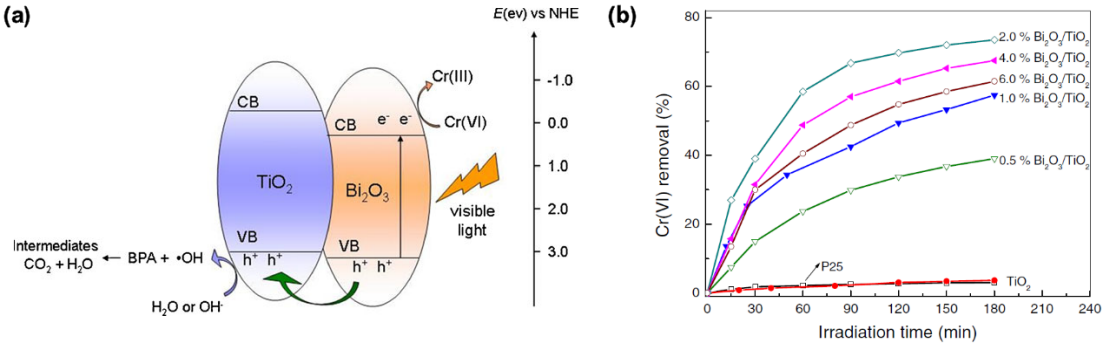

Figure 10. (**a**) Photocatalytic reduction of Cr(VI) and degradation of bisphenol A (BPA) in Bi_2O_3/TiO_2 system under visible-light irradiation; (**b**) photocatalytic reduction of Cr(VI) (20 mg/L) over Bi_2O_3/TiO_2 and P25 TiO_2 under visible light irradiation ($\lambda > 420$ nm). Reprinted with permission from [128]. Copyright 2012, Springer.

A palladium-modified nitrogen-doped titanium oxide (TiON/PdO) photocatalyst has been proposed for the photocatalytic disinfection of biological pollutants under visible light irradiation. PdO served as photoelectron trapping centres, thus reducing the e^-/h^+ pair recombination rate and increasing the lifetime of charge carriers, leading to much higher production of reactive oxidant species. In particular, this heterostructure is a very promising, environmentally friendly and cost-effective alternative method to treat blue algae in water. As reported by Wang et al., TiON/PdO has demonstrated superior photocatalytic disinfection efficiency on *Anabaena* sp. PCC 7120 under visible light illumination. Chlorophyll *a* content in blue algae cells has been completely removed by TiON/PdO nanoparticles after a few hours of visible light illumination. This result, in terms of the photocatalytic disinfection process, has mainly been attributed to the catalyst leakage, which caused severe damage on the cell wall/membrane of blue algae cells. TiON/PdO nanoparticles have also demonstrated a high photocatalytic degradation percentage of Microcystin LR under visible light illumination [130].

3.2. Photocatalytic Removal of Atmospheric Pollutants

The abundance of NO_x and VOCs (volatile organic compounds) in the atmosphere is an increasing environmental concern with harmful consequences not only for the environment, but also for human health. Their release in the atmosphere is mainly related to anthropogenic sources: combustion processes, fossil fuels, car exhausts, paints and coatings, cleaning products, refrigerants and furnishings. The removal of NO_x and VOCs is of paramount importance for both open and indoor air. In particular, people spend much of their time indoors, therefore long-term exposure to VOCs and NO_x in the indoor environment can contribute to "sick building syndrome" [131]. Unfortunately, UV-driven photocatalysis is not advisable for indoor application due to the adverse effect of UV light on human health upon long exposure. Therefore, there is increasing demand for photocatalysts able to exploit sunlight or commonly used visible light sources.

3.2.1. Photocatalytic Degradation of NO_x

NO_x denotes both nitrogen(II) oxide (NO) and nitrogen(IV) oxide (NO_2). In particular, during combustion processes, NO is generated and afterwards is oxidized to NO_2 by the atmospheric oxygen. Therefore, the largest contribution to total NO_x emissions is linked to anthropogenic activities including stationary power plants and automobile engines. The effects of NO_x on the environment include acid rain, photochemical smog, and ozone layer depletion; furthermore, increasing NO_x emissions produce an indirect impact on the greenhouse effect, as well as on human health. Several methods have been developed in order to decrease the production of NO. Primary methods involve the reduction of NO emissions inside a combustion zone, whereas secondary methods consist of catalytic and photocatalytic

processes. Among secondary methods, TiO_2-assisted photocatalysis is gaining increasing attention, as demonstrated by the huge number of commercial products and patented materials specifically designed for this application [9,132]. The photocatalytic NO_x removal occurs through subsequent oxidation reactions that ultimately lead to the production of HNO_3. The photocatalytic removal of NO_x, assisted by TiO_2, can also take place by photo-decomposition reactions that generate N_2 as the final product [132]. The examples reported in the literature on photocatalytic NO_x abatement make use of TiO_2 nanoparticles and UV light. Conversely, the applications of visible-light-active TiO_2-based heterostructures for photocatalytic NO_x removal are hardly reported. The present section will focus on TiO_2-based heterostructures, designed in order to effectively obtain photocatalytic NO_x removal under visible light. For this purpose, a system with coupled semiconductors has been prepared by Balbuena et al. In particular, a TiO_2/Fe_2O_3 heterojunction has been deposited on a silicon substrate by plasmochemical techniques and successfully applied for NO removal under visible light. The proposed heterostructure has been demonstrated to be more effective than TiO_2 P25 in the same experimental conditions. The authors have claimed that TiO_2/Fe_2O_3 has also shown increased selectivity towards HNO_3 (63%) compared to the benchmark TiO_2 P25 (25%). The effectiveness of the TiO_2/Fe_2O_3 heterostructure has been related to the twofold role played by Fe_2O_3: on one hand, it improves the visible light harvesting; on the other hand, it contributes to decreased e^-/h^+ recombination events [133].

Promising outcomes in the photocatalytic NO removal under visible light have been achieved by exploiting TiO_2-based heterostructures, modified with graphene oxide (TiO_2/GO) and surfactant-modified graphene (ssG/TiO_2). Both the heterostructures have provided NO_x removal efficiency two times higher than that of the unmodified TiO_2. Surprisingly, such improvement has not been ascribed to the higher surface area nor to the E_g of the heterostructures, but to the excellent ability of graphene to accumulate photogenerated electrons, thus improving charge separation [134]. A further example of the efficiency of the C-based TiO_2 heterostructures can be seen in the NO removal under visible light irradiation reported by Ma and co-workers. TiO_2 P25 modified with C_3N_4, by a solvothermal procedure, has displayed selectivity higher than that of the heterostructure prepared by the mechanical mixing of TiO_2 and C_3N_4. Such a result has highlighted the importance of effective interaction between TiO_2 and C_3N_4 for the preparation of a performant photocatalyst [135].

The integration of noble metal nanoparticles at the surface of TiO_2 nanocrystals has been a widely recognised and successful strategy for improving the photocatalytic activity of TiO_2 under both UV and visible light irradiation. In a very recent paper, TiO_2 modified with Ag nanoparticles has been investigated to promote the photocatalytic decomposition of NO to N_2. Interestingly, as in the case of C_3N_4/TiO_2 heterostructure, TiO_2/Ag has not shown higher NO removal but has displayed strong improvement in reaction selectivity and in particular in the conversion of NO to N_2. This is a crucial point because high selectivity means that the photocatalyst has not led to secondary pollution, generating harmful byproducts. The authors have shown that as the Ag loading decreases, the amount of photocatalytic conversion of NO to N_2 increases. Ag nanoparticles have been found to play two distinct functions: the first is to contribute to visible light harvesting thanks to the surface plasmon resonance phenomenon; the second is to provide a source of Ag^+ ions that interact with the byproduct N_2O, forming an Ag^+–N_2O complex that can be rapidly decomposed to N_2 [136].

3.2.2. Photocatalytic Degradation of VOCs

Polluting volatile organic compounds (VOCs) have been demonstrated to be involved in the production of tropospheric ozone and secondary organic aerosol. Many VOCs are toxic and carcinogenic. The most common VOCs are halogenated hydrocarbons, ketones, alcohols and aromatic compounds widely used in many industries, and are often found in the emissions. Photocatalytic processes assisted by TiO_2 surfaces may potentially remove VOCs, leading to benign and odourless constituents such as water vapour (H_2O) and carbon dioxide (CO_2) [2].

Demeestere et al. demonstrated the degradation of gaseous trichloroethylene (TCE) and dimethyl sulphide (DMS) in a batch reactor by CdS-modified TiO_2 under visible irradiation [137]. $LaVO_4/TiO_2$ heterostructures prepared by the sol-gel method have been reported to efficiently degrade benzene in the gaseous phase in a fixed-bed reactor under irradiation with a 500 W Xe arc lamp [138]. Efficient air purification has been proposed by Xiao et al. The $InVO_4$-modified mesoporous nanocrystalline TiO_2 heterostructures prepared by the sol-gel method and the degradation of up to five organic pollutants (e.g., benzene, toluene, cyclohexane, acetone and/or ethylbenzene) have been investigated under 500 W Xe arc lamp irradiation [139]. The degradation of acetone in the gas phase under a visible light supplied by Sunlite 8 W white LED lamp phase has been achieved by exploiting Bi_2WO_6-modified TiO_2 nanoparticles [140]. CNT/TiO_2 nanofibers have been integrated in a simulated air purifier. The heterostructure was irradiated under visible light (λ = 435 nm). Benzene vapour has been selected as a target compound, achieving 50% degradation after 120 min of irradiation [141]. Metallic copper nanoparticles have been exploited to decorate TiO_2 and to investigate the photocatalytic degradation of gaseous acetone and acetaldehyde under visible LED irradiation (400–700 nm). The authors reported a 27% degradation for acetone and 16% degradation for acetaldehyde after 6 h of irradiation [142,143].

3.3. Self-Cleaning Surfaces

Self-cleaning materials have gained considerable attention both for their unique properties and their practical applications in the energy and environmental fields. Such materials possess chemical and textural features inspired by nature: lotus leaves, butterfly wings and fish scales [144]. In particular, TiO_2 is an attractive material for its self-cleaning properties, which originate from a combination of the photocatalytic oxidative decomposition of organic contaminants and superhydrophilicity. The latter is induced by the generation of charged species at the TiO_2 surface upon irradiation, which causes water droplets to spread on the TiO_2 surface, thus favouring the cleaning process [145]. In order to improve the photocatalytic self-cleaning property in the visible region of the solar spectrum [146], several strategies have been reported in the literature, including the formation of hetero-junctions between TiO_2 and other low-bandgap semiconductors, modification of TiO_2 with metals and non-metals, and fabrication of graphene-based hybrid nanocatalysts.

Srinivasan et al. reported that a layered $TiO_2/WO_3/Pt$ thin film shows high photocatalytic activity to remove surface organic contaminants (stearic acid) and superhydrophilicity under visible light illumination. This material has been fabricated on a glass substrate by forming thin-layer TiO_2 on WO_3 with underlying Pt nanoparticles. In this case, a TiO_2 layer coated on WO_3 plays a dual role: as co-catalyst for an enhanced charge separation by hole transfer and as a protective layer to improve the chemical stability of WO_3 [147].

Tian et al. have synthesised hierarchical flake-like Bi_2MoO_6/TiO_2 bilayer films with controlled surface morphological structure by a facile solvothermal process. In this study, to evaluate the photocatalytic oxidative decomposition performance of the bilayer films, the degradation of alizarin red ARS (an anthraquinone dye) under visible light irradiation has been examined. Specifically, the Bi_2MoO_6/TiO_2 bilayer films exhibit a much higher (85%) photodegradation percentage of ARS than that of single-layer TiO_2 and Bi_2MoO_6 films. This significant visible-light self-cleaning performance could be attributed to the synergistic effect of a hierarchical flake-like porous surface with large surface area, superhydrophilicity, and effective charge separation due to the heterojunction interface between the two semiconductors [145].

Qiu et al. have reported that the Cu_xO/TiO_2 photocatalyst provides effective VOCs removal and antimicrobial activity in indoor environments. Specifically, the Cu^{II} species in the Cu_xO/TiO_2 improve the visible-light driven photo-oxidation of VOCs, whereas the Cu^{I} species provide antimicrobial properties under dark conditions. Such effective VOCs decomposition and antipathogenic activity have been attained in Cu_xO/TiO_2 heterostructures by tuning the ratio between Cu^{I} and Cu^{II} in Cu_xO [148].

Verbruggen et al. reported a plasmonic gold–silver alloy on the TiO_2 photocatalyst. In this case, $Au_{0.3}Ag_{0.7}$ nanoparticles on TiO_2 P90 (from Evonik, Essen, Germany) generate an SPR signal at 490 nm, which matched the intensity maximum of the solar spectrum. This material showed a higher degradation of stearic acid under the pure visible light (490 nm) illumination provided by LEDs than pristine TiO_2. Moreover, the ability to carefully control the light response of photoactive materials could lead to the development of more efficient solar-light-driven photocatalytic processes (Figure 11) [149].

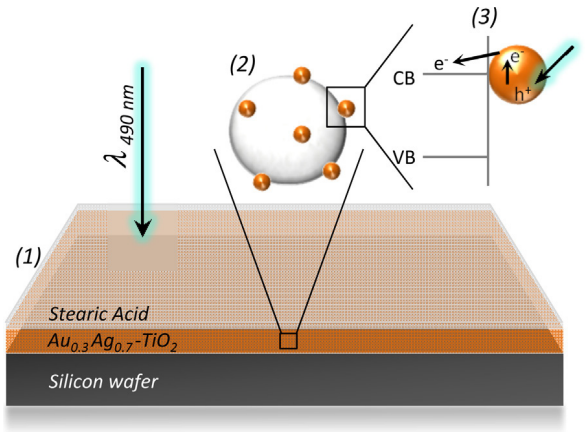

Figure 11. Schematic representation of the experimental setup: (1) a silicon wafer is coated with a layer of plasmonic photocatalyst and a solid layer of stearic acid is applied by spin coating. Experiments are conducted under visible light (490 nm) provided by LEDs. (2) Schematic representation of a plasmonic photocatalyst particle: noble metal alloy nanoparticles deposited on TiO_2 P90. (3) Schematic illustration of the charge transfer mechanism at the metal nanoparticle–TiO_2 interface. Reprinted with permission from [149]. Copyright 2014, Elsevier.

Recently, self-cleaning textiles (such as cotton, wool and polyester) with nano-photocatalyst coatings have attracted attention due to their potential applications at a large scale to make human life more convenient. TiO_2 or TiO_2/SiO_2 nanosols incorporating noble metals have been developed for cotton fabrics with visible-light-driven self-cleaning performance [150].

The $Au/TiO_2/SiO_2$-coated woven cotton fabrics reported by Wang et al. have demonstrated the removal of stains such as coffee and red wine. The $Au/TiO_2/SiO_2$ samples have shown significant visible-light self-cleaning performance in comparison to TiO_2 only-treatment. They have observed that the decolouration of a red wine stain in $Au/TiO_2/SiO_2$ is more significant after 20 h of irradiation in comparison with TiO_2-treated woven cotton fabrics, while both TiO_2 and $Au/TiO_2/SiO_2$ samples have shown significant decolouration of concentrated coffee stains after 20 h of visible light irradiation [151].

Furthermore, Pakdel et al. have studied the enhancement of photocatalytic activities using ternary TiO_2-based systems (TiO_2/metal/SiO_2) in textile applications. In this study, three types of noble metals, Pt, Au and Ag, have been incorporated into TiO_2 and TiO_2/SiO_2 colloids at different concentrations (Figure 12). Moreover, the photocatalytic activity of this material has been analysed by investigating coffee stain removal and MB degradation rates under visible light. The reported results demonstrate an enhancement in the photocatalytic activity upon metal nanoparticles' addition to the ternary system. Specifically, $TiO_2/Pt/SiO_2$30/1/70, $TiO_2/Au/SiO_2$30/0.1/70 along with $TiO_2/Ag/SiO_2$30/0.1/70, show the highest enhancement in self-cleaning properties of fabrics under visible light [152].

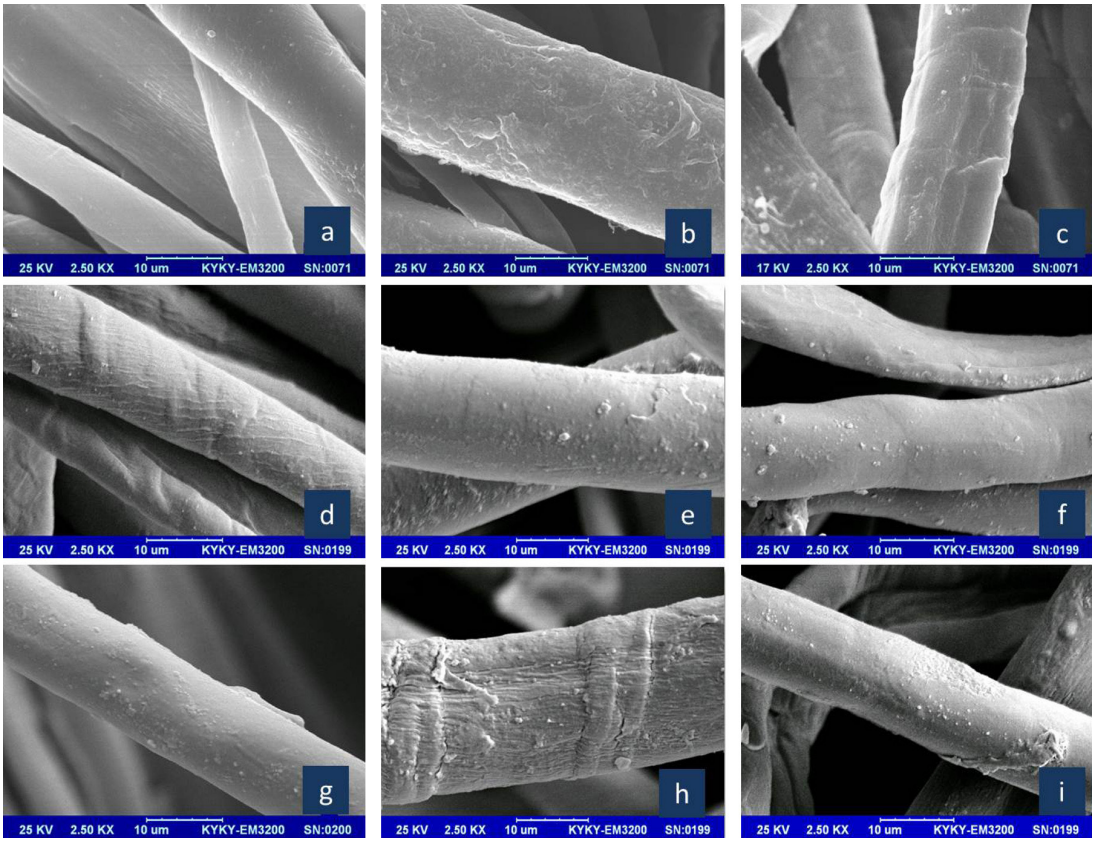

Figure 12. SEM images of cotton fabrics: (**a**) pristine cotton, cotton fabric coated with (**b**) TiO_2; (**c**) $TiO_2/SiO_2$30/70; (**d**) TiO_2/Au 0.1%; (**e**) TiO_2/Au/$SiO_2$30/0.1/70; (**f**) TiO_2/Pt 1%; (**g**) TiO_2/Pt/$SiO_2$30/1/70; (**h**) TiO_2/Ag 0.1% and (**i**) TiO_2/Ag/$SiO_2$30/0.1/70. Reprinted with permission from [152]. Copyright 2014, Elsevier.

In_2O_3/TiO_2 has been deposited by reactive sputtering onto polyester textiles for disinfection purpose (Figure 13). The samples have accelerated the *Escherichia coli* inactivation under actinic and simulated solar light. The experimental results shown that the fastest bacterial inactivation has been obtained for the TiO_2 10 min–In_2O_3 10 s sputtered sample. In particular, for this sample, the inactivation time has been reduced to 90 min by simulated sunlight irradiation with 50 mW/cm^2. In addition, thinner TiO_2–In_2O_3 coatings have led to bacterial inactivation faster than was found for TiO_2–In_2O_3 layers due to the reverse diffusion of the generated charges [153].

An electroconductive, self-cleaning, antibacterial and antifungal graphene/titanium dioxide-coated cotton fabric has been reported by Karimi et al. The cotton fabrics have been coated with graphene oxide, and later reduced by titanium trichloride obtaining graphene/titanium dioxide nanocomposite on the surface. The experimental results have indicated that, under sunlight irradiation, the graphene/TiO_2-treated samples showed a photocatalytic MB degradation efficiency up to 87%, while TiO_2-coated cotton showed slight MB degradation. Moreover, the graphene/titanium dioxide-coated cotton samples show negligible toxicity, while possessing antimicrobial activity [154].

Another brilliant system is a triple functional (self-cleaning, photocatalytic, thermochromic) nanomaterial with application in energy-saving smart windows. In particular, titania-vanadia systems have been studied extensively in the literature due to two advantageous properties, namely TiO_2 photocatalytic performance and the thermochromic characteristics of vanadium dioxide (VO_2). The film deposited on glass exhibited remarkable hydrophobicity, with the potential for self-cleaning under visible light. Furthermore, these materials show enhanced transmittance in the visible and near-infrared switching efficiency, similar to the behaviour of an antireflective coating [155].

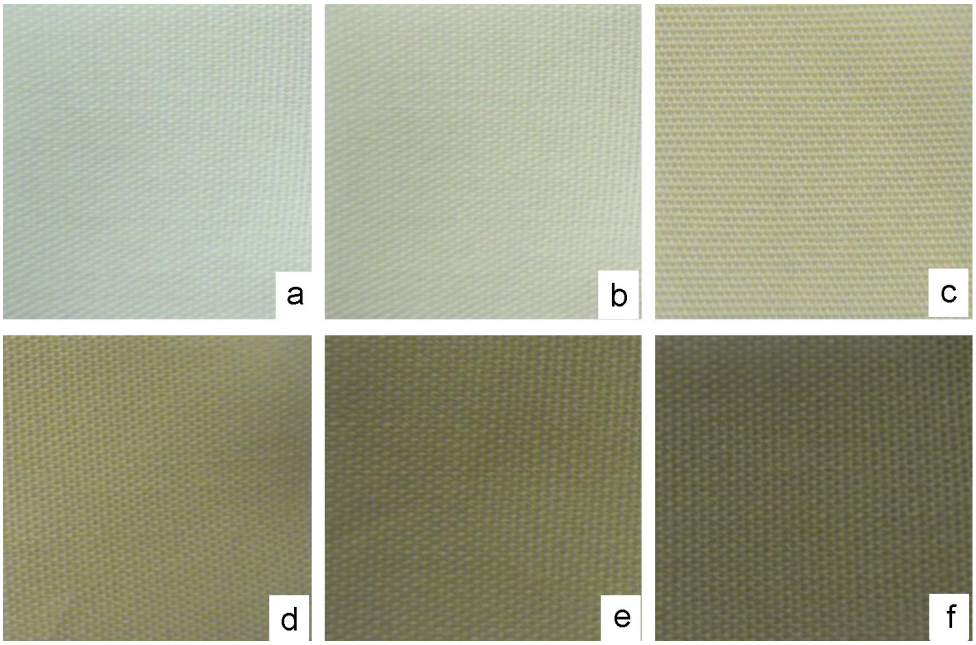

Figure 13. Pictures of the magnetron-sputtered polyester samples: (**a**) polyester alone; (**b**) $TiO_2$10 min; (**c**) TiO_2 10 min–In_2O_3 5 s; (**d**) TiO_2 10 min–In_2O_3 10 s; (**e**) TiO_2 10 min–In_2O_3 20 s; (**f**) TiO_2 10 min–In_2O_3 40 s. Reprinted with permission from [153]. Copyright 2014, Elsevier.

Moreover, manufactured nanomaterials and nanocomposites have been considered to advance conventional construction materials in the construction industry. The presence of nanomaterials can improve vital characteristics of construction materials such as strength, durability and lightness. Despite the high cost of these construction materials, their use in building applications is attributed to (1) highly valuable properties conveyed at relatively low additive loading; (2) rapid development of new applications exploiting particular nanomaterials' properties; (3) decreasing production cost of nanomaterials as their large-scale production increases [156].

Nevertheless, the benefits of incorporating nanomaterials in construction materials may be offset by concerns about their release into the environment as harmful contaminants, from the time of construction to demolition and disposal [156]. Such materials may transform over time via physical, chemical or biological processes. Unfortunately, few studies currently published have investigated the long-term physical and chemical changes of embedded nanomaterials and their associated hazards [157]. The use of these materials has already raised issues concerning their toxicity. Products containing nanoparticles should be labelled in order to facilitate future separation and recycling procedures [158].

A variety of nanomaterials can have beneficial applications in construction, such as concrete, steel, glass windows, pavement, walls, roofs, paint and coatings [156]. The integration of photocatalysts in building materials started from the early 1990s, with TiO_2 being one of the most widely used materials [159]. Embedding TiO_2 building materials provide several advantages: (1) relatively low cost and chemical stability; (2) high photocatalytic activity; (3) compatibility with conventional construction materials, such as cement, retaining their original performance; and (4) photoactivity even under weak solar irradiation in atmospheric environment [160].

Several applications of TiO_2 related to building materials have been reported in the literature, namely embedding in concrete, mortars, and ceramics, or exploited as a coating on glass and building stone surfaces. In recent years, TiO_2 has also proved promising for the conservation of stone in Cultural Heritage [161]. Indeed, photocatalysts applied as coatings on buildings and stone structures may

preserve the original appearance of the structures, slowing down degradation processes and thus reducing surface soiling and the need for costly cleaning operations [162,163].

Over the past 30 years, the enhancement of TiO_2 photocatalytic activity has been obtained through the addition of a metal dopant (such as Ag, Au, and Pt) and oxides (such as SiO_2, ZnO, etc.), thus improving self-cleaning and antibacterial properties [162]. Photocatalytic applications of visible active TiO_2-based nanoheterostructures already have a role in the fields of photocatalytic construction and building materials. However, due to their prohibitive cost and/or incompatibility with cementitious materials, their large-scale application in this field remains rather limited [164].

Among noble metals, Ag has been widely used owing to its high efficiency and its ability to provide tuneable surface plasmons in the visible spectral range. Pinho et al. synthesised $Ag/TiO_2/SiO_2$ photocatalysts suitable for outdoor application as self-cleaning and decontaminating coatings on stones and other building materials. This material has been applied on a pure limestone employed in both modern and ancient buildings. An SiO_2 matrix has been used for two reasons: (1) to avoid the oxidation of silver and tune the distance between silver and TiO_2 nanoparticles; and (2) to prevent the release of TiO_2 into the environment, thanks to the shielding action of the SiO_2 matrix that embeds the catalysts [163].

Specifically, the integration of high Ag loadings in a TiO_2–SiO_2 network (10% w/w) has been reported to significantly increase the photoactivity of a coating containing 1% (w/v) TiO_2 due to the improved visible light absorption and the high surface area of the photocatalyst. Another recent study reports that a nitrogen and carbon co-modified TiO_2 photocatalyst (TiO_2-N,C) can be implemented in cementitious materials to promote self-cleaning properties [165]. The self-cleaning properties of the prepared cement samples have been tested through the degradation of model organic compounds (Monoazo dye Reactive Red 198, RR 198) under UV-Vis light. The best self-cleaning properties have been found in cement plates containing 10 wt % of TiO_2/N, C-300 photocatalyst, after 100 h of UV-Vis light irradiation (Figure 14).

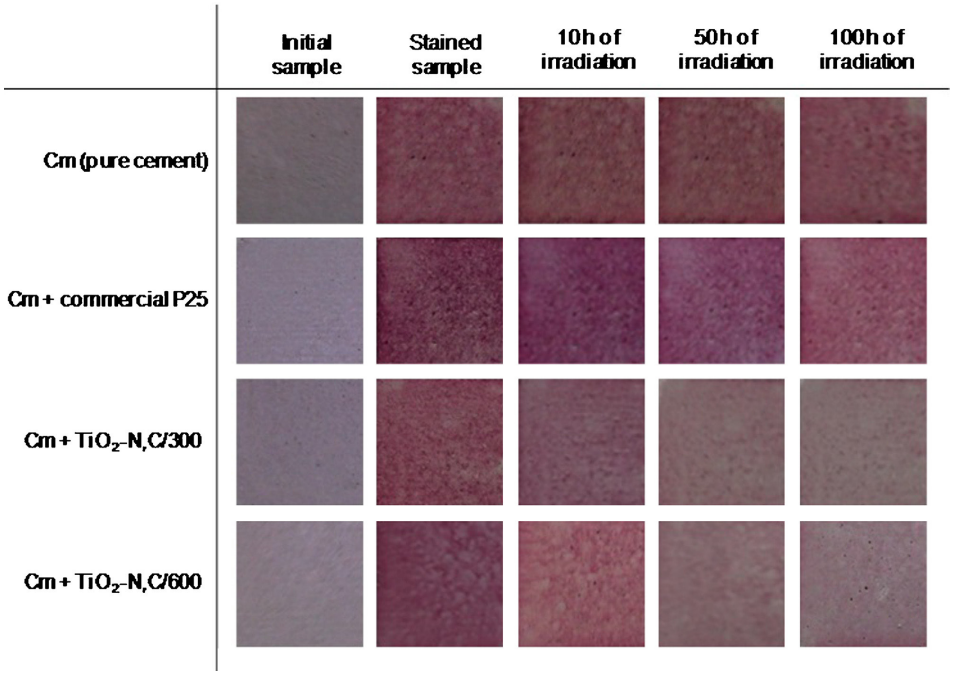

Figure 14. Photographs of pristine cement samples and samples stained with Reactive Red 198 (RR 198) dye taken after 10, 50 and 100 h of irradiated under UV–vis light source—the comparison of pure cement plates and exemplary cement plates containing 5 wt % of commercial P25 or TiO_2-N,C photocatalysts, calcined at 300 or 600 °C. Reprinted with permission from reference [165]. Copyright 2015, Elsevier.

4. Conclusions

Photocatalytically active hybrid nanomaterials, addressing the increasing demand of materials responsive to visible light, could pave the way toward large-scale application of photocatalysis for environmental remediation.

In the present review we have focused on those hybrid nanocrystals based on TiO_2, reporting several examples of synthetic procedures and discussing their potential in water remediation, the abatement of atmospheric pollutants (NO_x and VOCs) and their exploitation as self-cleaning materials. The survey of the literature has demonstrated the great progress achieved in the field of hybrid nanocrystal synthesis, offering the opportunity to precisely control the chemistry, geometry and chemical–physical properties of hybrid nanocrystals. Studies on the photocatalytic activity of such nanocatalysts, although showing that their large-scale application is still a challenge, indicate that such nanomaterials hold great promise for the degradation of organic and inorganic pollutants in the water or gas phase.

Acknowledgments: This work was partially supported by the Apulia Region Funded Projects NanoApulia (MDI6SR) and RELA-VALBIOR—Network of Laboratories for Scientific Research, by PON MAIND-PON03PE_00004_1 and by the National PRIN 2012—Prot. 2012T9XHH7 project.

Author Contributions: Roberto Comparelli conceived and drafted the work. Alessandra Truppi, Francesca Petronella and Tiziana Placido designed the article and acquired, analysed and interpreted the reports in the literature. Marinella Striccoli, Angela Agostiano and Maria Lucia Curri critically revised the manuscript.

Conflicts of Interest: The authors declare no conflict of interest. The founding sponsors had no role in the design of the study; in the collection, analyses, or interpretation of data; in the writing of the manuscript, and in the decision to publish the results.

References

1. Pelaez, M.; Nolan, N.T.; Pillai, S.C.; Seery, M.K.; Falaras, P.; Kontos, A.G.; Dunlop, P.S.M.; Hamilton, J.W.J.; Byrne, J.A.; O'Shea, K.; et al. A review on the visible light active titanium dioxide photocatalysts for environmental applications. *Appl. Catal. B* **2012**, *125*, 331–349. [CrossRef]
2. Petronella, F.; Truppi, A.; Ingrosso, C.; Placido, T.; Striccoli, M.; Curri, M.L.; Agostiano, A.; Comparelli, R. Nanocomposite materials for photocatalytic degradation of pollutants. *Catal. Today* **2017**, *281*, 85–100. [CrossRef]
3. Chen, X.; Mao, S.S. Titanium dioxide nanomaterials: Synthesis, properties, modifications, and applications. *Chem. Rev.* **2007**, *107*, 2891–2959. [CrossRef] [PubMed]
4. Chen, X.; Shen, S.; Guo, L.; Mao, S.S. Semiconductor-based photocatalytic hydrogen generation. *Chem. Rev.* **2010**, *110*, 6503–6570. [CrossRef] [PubMed]
5. Byrne, J.; Dunlop, P.; Hamilton, J.; Fernández-Ibáñez, P.; Polo-López, I.; Sharma, P.; Vennard, A. A review of heterogeneous photocatalysis for water and surface disinfection. *Molecules* **2015**, *20*, 5574. [CrossRef] [PubMed]
6. Ibhadon, A.; Fitzpatrick, P. Heterogeneous photocatalysis: Recent advances and applications. *Catalysts* **2013**, *3*, 189–218. [CrossRef]
7. Liao, C.-H.; Huang, C.-W.; Wu, J.C.S. Hydrogen production from semiconductor-based photocatalysis via water splitting. *Catalysts* **2012**, *2*, 490–516. [CrossRef]
8. Lazar, M.; Varghese, S.; Nair, S. Photocatalytic water treatment by titanium dioxide: Recent updates. *Catalysts* **2012**, *2*, 572–601. [CrossRef]
9. Paz, Y. Application of TiO_2 photocatalysis for air treatment: Patents' overview. *Appl. Catal. B* **2010**, *99*, 448–460. [CrossRef]
10. Kiwi, J.; Pulgarin, C. Innovative self-cleaning and bactericide textiles. *Catal. Today* **2010**, *151*, 2–7. [CrossRef]
11. Petronella, F.; Pagliarulo, A.; Striccoli, M.; Calia, A.; Lettieri, M.; Colangiuli, D.; Curri, M.; Comparelli, R. Colloidal nanocrystalline semiconductor materials as photocatalysts for environmental protection of architectural stone. *Crystals* **2017**, *7*, 30. [CrossRef]

12. Comparelli, R.; Fanizza, E.; Curri, M.L.; Cozzoli, P.D.; Mascolo, G.; Passino, R.; Agostiano, A. Photocatalytic degradation of azo dyes by organic-capped anatase TiO_2 nanocrystals immobilized onto substrates. *Appl. Catal. B* **2005**, *55*, 81–91. [CrossRef]
13. Fittipaldi, M.; Curri, M.L.; Comparelli, R.; Striccoli, M.; Agostiano, A.; Grassi, N.; Sangregorio, C.; Gatteschi, D. A multifrequency EPR study on organic-capped anatase TiO_2 nanocrystals. *J. Phys. Chem. C* **2009**, *113*, 6221–6226. [CrossRef]
14. Panniello, A.; Curri, M.L.; Diso, D.; Licciulli, A.; Locaputo, V.; Agostiano, A.; Comparelli, R.; Mascolo, G. Nanocrystalline TiO_2 based films onto fibers for photocatalytic degradation of organic dye in aqueous solution. *Appl. Catal. B* **2012**, *121–122*, 190–197. [CrossRef]
15. Linsebigler, A.L.; Lu, G.; Yates, J.T. Photocatalysis on TiO_2 surfaces: Principles, mechanisms, and selected results. *Chem. Rev.* **1995**, *95*, 735–758. [CrossRef]
16. Zhou, N.; Lopez-Puente, V.; Wang, Q.; Polavarapu, L.; Pastoriza-Santos, I.; Xu, Q.-H. Plasmon-enhanced light harvesting: Applications in enhanced photocatalysis, photodynamic therapy and photovoltaics. *RSC Adv.* **2015**, *5*, 29076–29097. [CrossRef]
17. Petronella, F.; Curri, M.L.; Striccoli, M.; Fanizza, E.; Mateo-Mateo, C.; Alvarez-Puebla, R.A.; Sibillano, T.; Giannini, C.; Correa-Duarte, M.A.; Comparelli, R. Direct growth of shape controlled TiO_2 nanocrystals onto SWCNTs for highly active photocatalytic materials in the visible. *Appl. Catal. B* **2015**, *178*, 91–99. [CrossRef]
18. Ben-Shahar, Y.; Banin, U. Hybrid semiconductor–metal nanorods as photocatalysts. *Top. Curr. Chem.* **2016**, *374*, 54. [CrossRef] [PubMed]
19. Murgolo, S.; Petronella, F.; Ciannarella, R.; Comparelli, R.; Agostiano, A.; Curri, M.L.; Mascolo, G. UV and solar-based photocatalytic degradation of organic pollutants by nano-sized TiO_2 grown on carbon nanotubes. *Catal. Today* **2015**, *240*, 114–124. [CrossRef]
20. Petronella, F.; Truppi, A.; Sibillano, T.; Giannini, C.; Striccoli, M.; Comparelli, R.; Curri, M.L. Multifunctional $TiO_2/Fe_xO_y/Ag$ based nanocrystalline heterostructures for photocatalytic degradation of a recalcitrant pollutant. *Catal. Today* **2016**. [CrossRef]
21. Carbone, L.; Cozzoli, P.D. Colloidal heterostructured nanocrystals: Synthesis and growth mechanisms. *Nano Today* **2010**, *5*, 449–493. [CrossRef]
22. Casavola, M.; Buonsanti, R.; Caputo, G.; Cozzoli, P.D. Colloidal strategies for preparing oxide-based hybrid nanocrystals. *Eur. J. Inorg. Chem.* **2008**, *2008*, 837–854. [CrossRef]
23. Cozzoli, P.D.; Pellegrino, T.; Manna, L. Synthesis, properties and perspectives of hybrid nanocrystal structures. *Chem. Soc. Rev.* **2006**, *35*, 1195–1208. [CrossRef] [PubMed]
24. Wang, Y.; Zheng, Y.-Z.; Lu, S.; Tao, X.; Che, Y.; Chen, J.-F. Visible-light-responsive TiO_2-coated ZnO:I nanorod array films with enhanced photoelectrochemical and photocatalytic performance. *ACS Appl. Mater. Interfaces* **2015**, *7*, 6093–6101. [CrossRef] [PubMed]
25. Manthina, V.; Correa Baena, J.P.; Liu, G.; Agrios, A.G. ZnO–TiO_2 nanocomposite films for high light harvesting efficiency and fast electron transport in dye-sensitized solar cells. *J. Phys. Chem. C* **2012**, *116*, 23864–23870. [CrossRef]
26. Costi, R.; Saunders, A.E.; Banin, U. Colloidal hybrid nanostructures: A new type of functional materials. *Angew. Chem. Int. Ed.* **2010**, *49*, 4878–4897. [CrossRef] [PubMed]
27. Wang, H.; Zhang, L.; Chen, Z.; Hu, J.; Li, S.; Wang, Z.; Liu, J.; Wang, X. Semiconductor heterojunction photocatalysts: Design, construction, and photocatalytic performances. *Chem. Soc. Rev.* **2014**, *43*, 5234–5244. [CrossRef] [PubMed]
28. Daghrir, R.; Drogui, P.; Robert, D. Modified TiO_2 for environmental photocatalytic applications: A review. *Ind. Eng. Chem. Res.* **2013**, *52*, 3581–3599. [CrossRef]
29. Yang, L.; Luo, S.; Li, Y.; Xiao, Y.; Kang, Q.; Cai, Q. High efficient photocatalytic degradation of p-nitrophenol on a unique Cu_2O/TiO_2 p-n heterojunction network catalyst. *Environ. Sci. Technol.* **2010**, *44*, 7641–7646. [CrossRef] [PubMed]
30. Wei, L.; Shifu, C.; Sujuan, Z.; Wei, Z.; Huaye, Z.; Xiaoling, Y. Preparation and characterization of p-n heterojunction photocatalyst p-$CuBi_2O_4$/n-TiO_2 with high photocatalytic activity under visible and UV light irradiation. *J. Nanopart. Res.* **2010**, *12*, 1355–1366. [CrossRef]
31. Lee, J.H.; Kim, S.-I.; Park, S.-M.; Kang, M. A p-n heterojunction NiS-sensitized TiO_2 photocatalytic system for efficient photoreduction of carbon dioxide to methane. *Ceram. Int.* **2017**, *43*, 1768–1774. [CrossRef]

32. Chen, C.; Cai, W.; Long, M.; Zhou, B.; Wu, Y.; Wu, D.; Feng, Y. Synthesis of visible-light responsive graphene oxide/TiO_2 composites with p/n heterojunction. *ACS Nano* **2010**, *4*, 6425–6432. [CrossRef] [PubMed]
33. Yang, G.; Yang, B.; Xiao, T.; Yan, Z. One-step solvothermal synthesis of hierarchically porous nanostructured CdS/TiO_2 heterojunction with higher visible light photocatalytic activity. *Appl. Surf. Sci.* **2013**, *283*, 402–410. [CrossRef]
34. Mu, J.; Chen, B.; Zhang, M.; Guo, Z.; Zhang, P.; Zhang, Z.; Sun, Y.; Shao, C.; Liu, Y. Enhancement of the visible-light photocatalytic activity of In_2O_3–TiO_2 nanofiber heteroarchitectures. *ACS Appl. Mater. Interfaces* **2011**, *4*, 424–430. [CrossRef] [PubMed]
35. Ren, G.; Gao, Y.; Yin, J.; Xing, A.; Liu, H. Synthesis of high activity TiO_2/WO_3 photocatalyst via environmentally friendly and microwave assisted hydrothermal process. *J. Chem. Soc. Pak.* **2011**, *33*, 666–679.
36. Kuang, S.; Yang, L.; Luo, S.; Cai, Q. Fabrication, characterization and photoelectrochemical properties of Fe_2O_3 modified TiO_2 nanotube arrays. *Appl. Surf. Sci.* **2009**, *255*, 7385–7388. [CrossRef]
37. Dahl, M.; Liu, Y.; Yin, Y. Composite titanium dioxide nanomaterials. *Chem. Rev.* **2014**, *114*, 9853–9889. [CrossRef] [PubMed]
38. Sajjad, A.K.L.; Shamaila, S.; Tian, B.; Chen, F.; Zhang, J. Comparative studies of operational parameters of degradation of azo dyes in visible light by highly efficient WO_x/TiO_2 photocatalyst. *J. Hazard. Mater.* **2010**, *177*, 781–791. [CrossRef] [PubMed]
39. Li, J.; Guo, Z.; Yu, W.; Zhu, Z. Three-dimensional TiO_2/Bi_2WO_6 hierarchical heterostructure with enhanced visible photocatalytic activity. *IET Micro Nano Lett.* **2014**, *9*, 65–68.
40. Li, S.; Lin, Y.-H.; Zhang, B.-P.; Li, J.-F.; Nan, C.-W. $BiFeO_3$/TiO_2 core-shell structured nanocomposites as visible-active photocatalysts and their optical response mechanism. *J. Appl. Phys.* **2009**, *105*, 054310. [CrossRef]
41. Li, X.; Hou, Y.; Zhao, Q.; Chen, G. Synthesis and photoinduced charge-transfer properties of a $ZnFe_2O_4$-sensitized TiO_2 nanotube array electrode. *Langmuir* **2011**, *27*, 3113–3120. [CrossRef] [PubMed]
42. Bi, F.; Ehsan, M.F.; Liu, W.; He, T. Visible-light photocatalytic conversion of carbon dioxide into methane using Cu_2O/TiO_2 hollow nanospheres. *Chin. J. Chem.* **2015**, *33*, 112–118. [CrossRef]
43. Liu, S.; Zhang, N.; Tang, Z.-R.; Xu, Y.-J. Synthesis of one-dimensional CdS@TiO_2 core–shell nanocomposites photocatalyst for selective redox: The dual role of TiO_2 shell. *ACS Appl. Mater. Interfaces* **2012**, *4*, 6378–6385. [CrossRef] [PubMed]
44. Wei, Z.; Li, Y.; Luo, S.; Liu, C.; Meng, D.; Ding, M.; Zeng, G. Hierarchical heterostructure of CdS nanoparticles sensitized electrospun TiO_2 nanofibers with enhanced photocatalytic activity. *Sep. Purif. Technol.* **2014**, *122*, 60–66. [CrossRef]
45. He, H.Y. Facile synthesis of ultrafine CuS nanocrystalline/TiO_2: Fe nanotubes hybrids and their photocatalytic and Fenton-like photocatalytic activities in the dye degradation. *Microporous Mesoporous Mater.* **2016**, *227*, 31–38. [CrossRef]
46. Lu, Y.Y.; Zhang, Y.Y.; Zhang, J.; Shi, Y.; Li, Z.; Feng, Z.C.; Li, C. In situ loading of CuS nanoflowers on rutile TiO_2 surface and their improved photocatalytic performance. *Appl. Surf. Sci.* **2016**, *370*, 312–319. [CrossRef]
47. Liu, B.; Li, X.; Zhao, Q.; Ke, J.; Tadé, M.; Liu, S. Preparation of $AgInS_2$/TiO_2 composites for enhanced photocatalytic degradation of gaseous o-dichlorobenzene under visible light. *Appl. Catal. B* **2016**, *185*, 1–10. [CrossRef]
48. Hou, W.; Cronin, S.B. A review of surface plasmon resonance-enhanced photocatalysis. *Adv. Funct. Mater.* **2013**, *23*, 1612–1619. [CrossRef]
49. De Sio, L.; Placido, T.; Comparelli, R.; Lucia Curri, M.; Striccoli, M.; Tabiryan, N.; Bunning, T.J. Next-generation thermo-plasmonic technologies and plasmonic nanoparticles in optoelectronics. *Prog. Quantum Electron.* **2015**, *41*, 23–70. [CrossRef]
50. Placido, T.; Aragay, G.; Pons, J.; Comparelli, R.; Curri, M.L.; Merkoçi, A. Ion-directed assembly of gold nanorods: A strategy for mercury detection. *ACS Appl. Mater. Interfaces* **2013**, *5*, 1084–1092. [CrossRef] [PubMed]
51. Placido, T.; Comparelli, R.; Giannici, F.; Cozzoli, P.D.; Capitani, G.; Striccoli, M.; Agostiano, A.; Curri, M.L. Photochemical synthesis of water-soluble gold nanorods: The role of silver in assisting anisotropic growth. *Chem. Mater.* **2009**, *21*, 4192–4202. [CrossRef]

52. Okuno, Y.; Nishioka, K.; Kiya, A.; Nakashima, N.; Ishibashi, A.; Niidome, Y. Uniform and controllable preparation of Au-Ag core–shell nanorods using anisotropic silver shell formation on gold nanorods. *Nanoscale* **2010**, *2*, 1489–1493. [CrossRef] [PubMed]
53. Chen, H.; Kou, X.; Yang, Z.; Ni, W.; Wang, J. Shape- and size-dependent refractive index sensitivity of gold nanoparticles. *Langmuir* **2008**, *24*, 5233–5237. [CrossRef] [PubMed]
54. Zhu, J. Shape dependent full width at half maximum of the absorption band in gold nanorods. *Phys. Lett. A* **2005**, *339*, 466–471. [CrossRef]
55. Comparelli, R.; Placido, T.; Depalo, N.; Fanizza, E.; Striccoli, M.; Curri, M.L. *Active Plasmonic Nanomaterials*; Pan Stanford Publishing: Boca Raton, FL, USA, 2015; pp. 33–100.
56. Hirakawa, T.; Kamat, P.V. Charge separation and catalytic activity of Ag@TiO_2 core–shell composite clusters under UV–irradiation. *J. Am. Chem. Soc.* **2005**, *127*, 3928–3934. [CrossRef] [PubMed]
57. Zhu, H.; Chen, X.; Zheng, Z.; Ke, X.; Jaatinen, E.; Zhao, J.; Guo, C.; Xie, T.; Wang, D. Mechanism of supported gold nanoparticles as photocatalysts under ultraviolet and visible light irradiation. *Chem. Commun.* **2009**. [CrossRef] [PubMed]
58. Arabatzis, I.M.; Stergiopoulos, T.; Andreeva, D.; Kitova, S.; Neophytides, S.G.; Falaras, P. Characterization and photocatalytic activity of Au/TiO_2 thin films for azo-dye degradation. *J. Catal.* **2003**, *220*, 127–135. [CrossRef]
59. Bumajdad, A.; Madkour, M. Understanding the superior photocatalytic activity of noble metals modified titania under UV and visible light irradiation. *Phys. Chem. Chem. Phys.* **2014**, *16*, 7146–7158. [CrossRef] [PubMed]
60. Zhang, X.; Zhu, Y.; Yang, X.; Wang, S.; Shen, J.; Lin, B.; Li, C. Enhanced visible light photocatalytic activity of interlayer-isolated triplex Ag@SiO_2@TiO_2 core–shell nanoparticles. *Nanoscale* **2013**, *5*, 3359–3366. [CrossRef] [PubMed]
61. Odom, T.W.; Schatz, G.C. Introduction to plasmonics. *Chem. Rev.* **2011**, *111*, 3667–3668. [CrossRef] [PubMed]
62. Kowalska, E.; Mahaney, O.O.P.; Abe, R.; Ohtani, B. Visible-light-induced photocatalysis through surface plasmon excitation of gold on titania surfaces. *Phys. Chem. Chem. Phys.* **2010**, *12*, 2344–2355. [CrossRef] [PubMed]
63. Della Gaspera, E.; Bersani, M.; Mattei, G.; Nguyen, T.-L.; Mulvaney, P.; Martucci, A. Cooperative effect of Au and Pt inside TiO_2 matrix for optical hydrogen detection at room temperature using surface plasmon spectroscopy. *Nanoscale* **2012**, *4*, 5972–5979. [CrossRef] [PubMed]
64. Hou, W.; Hung, W.H.; Pavaskar, P.; Goeppert, A.; Aykol, M.; Cronin, S.B. Photocatalytic conversion of CO_2 to hydrocarbon fuels via plasmon-enhanced absorption and metallic interband transitions. *ACS Catal.* **2011**, *1*, 929–936. [CrossRef]
65. Kumar, M.K.; Krishnamoorthy, S.; Tan, L.K.; Chiam, S.Y.; Tripathy, S.; Gao, H. Field effects in plasmonic photocatalyst by precise SiO_2 thickness control using atomic layer deposition. *ACS Catal.* **2011**, *1*, 300–308. [CrossRef]
66. Takai, A.; Kamat, P.V. Capture, store, and discharge. shuttling photogenerated electrons across TiO_2–silver interface. *ACS Nano* **2011**, *5*, 7369–7376. [CrossRef] [PubMed]
67. Zhou, N.; Polavarapu, L.; Gao, N.; Pan, Y.; Yuan, P.; Wang, Q.; Xu, Q.-H. TiO_2 coated Au/Ag nanorods with enhanced photocatalytic activity under visible light irradiation. *Nanoscale* **2013**, *5*, 4236–4241. [CrossRef] [PubMed]
68. Kmetykó, Á.; Szániel, Á.; Tsakiroglou, C.; Dombi, A.; Hernádi, K. Enhanced photocatalytic H_2 generation on noble metal modified TiO_2 catalysts excited with visible light irradiation. *React. Kinet. Mech. Catal.* **2016**, *117*, 379–390. [CrossRef]
69. Su, R.; Tiruvalam, R.; He, Q.; Dimitratos, N.; Kesavan, L.; Hammond, C.; Lopez-Sanchez, J.A.; Bechstein, R.; Kiely, C.J.; Hutchings, G.J.; et al. Promotion of phenol photodecomposition over TiO_2 using Au, Pd, and Au–Pd nanoparticles. *ACS Nano* **2012**, *6*, 6284–6292. [CrossRef] [PubMed]
70. Francioso, L.; Presicce, D.S.; Siciliano, P.; Ficarella, A. Combustion conditions discrimination properties of Pt-doped TiO_2 thin film oxygen sensor. *Sens. Actuators B* **2007**, *123*, 516–521. [CrossRef]
71. Mizukoshi, Y.; Makise, Y.; Shuto, T.; Hu, J.; Tominaga, A.; Shironita, S.; Tanabe, S. Immobilization of noble metal nanoparticles on the surface of TiO_2 by the sonochemical method: Photocatalytic production of hydrogen from an aqueous solution of ethanol. *Ultrason. Sonochem.* **2007**, *14*, 387–392. [CrossRef] [PubMed]

72. Wang, H.; You, T.; Shi, W.; Li, J.; Guo, L. Au/TiO_2/Au as a plasmonic coupling photocatalyst. *J. Phys. Chem. C* **2012**, *116*, 6490–6494. [CrossRef]
73. Sonawane, R.S.; Dongare, M.K. Sol-gel synthesis of Au/TiO_2 thin films for photocatalytic degradation of phenol in sunlight. *J. Mol. Catal. A* **2006**, *243*, 68–76. [CrossRef]
74. Chiarello, G.L.; Selli, E.; Forni, L. Photocatalytic hydrogen production over flame spray pyrolysis-synthesised TiO_2 and Au/TiO_2. *Appl. Catal. B* **2008**, *84*, 332–339. [CrossRef]
75. Damato, T.C.; de Oliveira, C.C.S.; Ando, R.A.; Camargo, P.H.C. A facile approach to TiO_2 colloidal spheres decorated with Au nanoparticles displaying well-defined sizes and uniform dispersion. *Langmuir* **2013**, *29*, 1642–1649. [CrossRef] [PubMed]
76. Iliev, V.; Tomova, D.; Bilyarska, L.; Tyuliev, G. Influence of the size of gold nanoparticles deposited on TiO_2 upon the photocatalytic destruction of oxalic acid. *J. Mol. Catal. A* **2007**, *263*, 32–38. [CrossRef]
77. Sakthivel, S.; Shankar, M.V.; Palanichamy, M.; Arabindoo, B.; Bahnemann, D.W.; Murugesan, V. Enhancement of photocatalytic activity by metal deposition: Characterisation and photonic efficiency of Pt, Au and Pd deposited on TiO_2 catalyst. *Water Res.* **2004**, *38*, 3001–3008. [CrossRef] [PubMed]
78. Kimling, J.; Maier, M.; Okenve, B.; Kotaidis, V.; Ballot, H.; Plech, A. Turkevich method for gold nanoparticle synthesis revisited. *J. Phys. Chem. B* **2006**, *110*, 15700–15707. [CrossRef] [PubMed]
79. Brust, M.; Walker, M.; Bethell, D.; Schiffrin, D.J.; Whyman, R. Synthesis of thiol-derivatised gold nanoparticles in a two-phase liquid-liquid system. *J. Chem. Soc. Chem. Commun.* **1994**. [CrossRef]
80. Bian, Z.; Zhu, J.; Cao, F.; Lu, Y.; Li, H. In situ encapsulation of Au nanoparticles in mesoporous core-shell TiO_2 microspheres with enhanced activity and durability. *Chem. Commun.* **2009**. [CrossRef] [PubMed]
81. Gomes Silva, C.; Juárez, R.; Marino, T.; Molinari, R.; García, H. Influence of excitation wavelength (UV or visible light) on the photocatalytic activity of titania containing gold nanoparticles for the generation of hydrogen or oxygen from water. *J. Am. Chem. Soc.* **2011**, *133*, 595–602. [CrossRef] [PubMed]
82. Zhang, N.; Liu, S.; Xu, Y.-J. Recent progress on metal core@semiconductor shell nanocomposites as a promising type of photocatalyst. *Nanoscale* **2012**, *4*, 2227–2238. [CrossRef] [PubMed]
83. Petronella, F.; Fanizza, E.; Mascolo, G.; Locaputo, V.; Bertinetti, L.; Martra, G.; Coluccia, S.; Agostiano, A.; Curri, M.L.; Comparelli, R. Photocatalytic activity of nanocomposite catalyst films based on nanocrystalline metal/semiconductors. *J. Phys. Chem. C* **2011**, *115*, 12033–12040. [CrossRef]
84. Kowalska, E.; Yoshiiri, K.; Wei, Z.; Zheng, S.; Kastl, E.; Remita, H.; Ohtani, B.; Rau, S. Hybrid photocatalysts composed of titania modified with plasmonic nanoparticles and ruthenium complexes for decomposition of organic compounds. *Appl. Catal. B* **2015**, *178*, 133–143. [CrossRef]
85. Cozzoli, P.D.; Comparelli, R.; Fanizza, E.; Curri, M.L.; Agostiano, A.; Laub, D. Photocatalytic synthesis of silver nanoparticles stabilized by TiO_2 nanorods: A semiconductor/metal nanocomposite in homogeneous nonpolar solution. *J. Am. Chem. Soc.* **2004**, *126*, 3868–3879. [CrossRef] [PubMed]
86. Cozzoli, P.D.; Curri, M.L.; Giannini, C.; Agostiano, A. Synthesis of TiO_2-Au composites by titania-nanorod-assisted generation of gold nanoparticles at aqueous/nonpolar interfaces. *Small* **2006**, *2*, 413–421. [CrossRef] [PubMed]
87. Chen, L.; Yang, S.; Hao, B.; Ruan, J.; Ma, P.-C. Preparation of fiber-based plasmonic photocatalyst and its photocatalytic performance under the visible light. *Appl. Catal. B* **2015**, *166–167*, 287–294. [CrossRef]
88. Murcia, J.J.; Ávila-Martínez, E.G.; Rojas, H.; Navío, J.A.; Hidalgo, M.C. Study of the *E. coli* elimination from urban wastewater over photocatalysts based on metallized TiO_2. *Appl. Catal. B* **2017**, *200*, 469–476. [CrossRef]
89. Buonsanti, R.; Grillo, V.; Carlino, E.; Giannini, C.; Curri, M.L.; Innocenti, C.; Sangregorio, C.; Achterhold, K.; Parak, F.G.; Agostiano, A.; et al. Seeded growth of asymmetric binary nanocrystals made of a semiconductor TiO_2 rodlike section and a magnetic γ-Fe_2O_3 spherical domain. *J. Am. Chem. Soc.* **2006**, *128*, 16953–16970. [CrossRef] [PubMed]
90. Lekeufack, D.D.; Brioude, A.; Mouti, A.; Alauzun, J.G.; Stadelmann, P.; Coleman, A.W.; Miele, P. Core-shell Au@(TiO_2, SiO_2) nanoparticles with tunable morphology. *Chem. Commun.* **2010**, *46*, 4544–4546. [CrossRef] [PubMed]
91. Pastoriza-Santos, I.; Koktysh, D.S.; Mamedov, A.A.; Giersig, M.; Kotov, N.A.; Liz-Marzán, L.M. One-pot synthesis of Ag@TiO_2 core–shell nanoparticles and their layer-by-layer assembly. *Langmuir* **2000**, *16*, 2731–2735. [CrossRef]

92. Mayya, K.S.; Gittins, D.I.; Caruso, F. Gold–titania core–shell nanoparticles by polyelectrolyte complexation with a titania precursor. *Chem. Mater.* **2001**, *13*, 3833–3836. [CrossRef]
93. Zhang, N.; Liu, S.; Fu, X.; Xu, Y.-J. Synthesis of M@TiO_2 (M = Au, Pd, Pt) core–shell nanocomposites with tunable photoreactivity. *J. Phys. Chem. C*, **2011**, *115*, 9136–9145. [CrossRef]
94. Horiguchi, Y.; Kanda, T.; Torigoe, K.; Sakai, H.; Abe, M. Preparation of gold/silver/titania trilayered nanorods and their photocatalytic activities. *Langmuir* **2014**, *30*, 922–928. [CrossRef] [PubMed]
95. Wu, B.; Liu, D.; Mubeen, S.; Chuong, T.T.; Moskovits, M.; Stucky, G.D. Anisotropic growth of TiO_2 onto gold nanorods for plasmon-enhanced hydrogen production from water reduction. *J. Am. Chem. Soc.* **2016**, *138*, 1114–1117. [CrossRef] [PubMed]
96. Kou, S.F.; Ye, W.; Guo, X.; Xu, X.F.; Sun, H.Y.; Yang, J. Gold nanorods coated by oxygen-deficient TiO_2 as an advanced photocatalyst for hydrogen evolution. *RSC Adv.* **2016**, *6*, 39144–39149. [CrossRef]
97. Jin, Z.; Wang, F.; Wang, F.; Wang, J.; Yu, J.C.; Wang, J. Metal nanocrystal-embedded hollow mesoporous TiO_2 and ZrO_2 microspheres prepared with polystyrene nanospheres as carriers and templates. *Adv. Funct. Mater.* **2013**, *23*, 2137–2144. [CrossRef]
98. Nikoobakht, B.; El-Sayed, M.A. Preparation and growth mechanism of gold nanorods (NRs) using seed-mediated growth method. *Chem. Mater.* **2003**, *15*, 1957–1962. [CrossRef]
99. Yang, K.; Meng, C.; Lin, L.; Peng, X.; Chen, X.; Wang, X.; Dai, W.; Fu, X. A heterostructured TiO_2-C_3N_4 support for gold catalysts: A superior preferential oxidation of CO in the presence of H_2 under visible light irradiation and without visible light irradiation. *Catal. Sci. Technol.* **2016**, *6*, 829–839. [CrossRef]
100. Chen, Q.; Wu, S.; Xin, Y. Synthesis of Au–CuS–TiO_2 nanobelts photocatalyst for efficient photocatalytic degradation of antibiotic oxytetracycline. *Chem. Eng. J.* **2016**, *302*, 377–387. [CrossRef]
101. Gao, W.; Wang, M.; Ran, C.; Yao, X.; Yang, H.; Liu, J.; He, D.; Bai, J. One-pot synthesis of Ag/r-GO/TiO_2 nanocomposites with high solar absorption and enhanced anti-recombination in photocatalytic applications. *Nanoscale* **2014**, *6*, 5498–5508. [CrossRef] [PubMed]
102. Hintsho, N.; Petrik, L.; Nechaev, A.; Titinchi, S.; Ndungu, P. Photo-catalytic activity of titanium dioxide carbon nanotube nano-composites modified with silver and palladium nanoparticles. *Appl. Catal. B* **2014**, *156–157*, 273–283. [CrossRef]
103. Wang, Y.; Pan, F.; Dong, W.; Xu, L.; Wu, K.; Xu, G.; Chen, W. Recyclable silver-decorated magnetic titania nanocomposite with enhanced visible-light photocatalytic activity. *Appl. Catal. B* **2016**, *189*, 192–198. [CrossRef]
104. Tang, Y.; Zhang, G.; Liu, C.; Luo, S.; Xu, X.; Chen, L.; Wang, B. Magnetic TiO_2-graphene composite as a high-performance and recyclable platform for efficient photocatalytic removal of herbicides from water. *J. Hazard. Mater.* **2013**, *252–253*, 115–122. [CrossRef] [PubMed]
105. Xu, J.-W.; Gao, Z.-D.; Han, K.; Liu, Y.; Song, Y.-Y. Synthesis of magnetically separable Ag_3PO_4/TiO_2/Fe_3O_4 heterostructure with enhanced photocatalytic performance under visible light for photoinactivation of bacteria. *ACS Appl. Mater. Interfaces* **2014**, *6*, 15122–15131. [PubMed]
106. Ma, S.; Zhan, S.; Jia, Y.; Zhou, Q. Superior antibacterial activity of Fe_3O_4-TiO_2 nanosheets under solar light. *ACS Appl. Mater. Interfaces* **2015**, *7*, 21875–21883. [CrossRef] [PubMed]
107. Leng, C.; Wei, J.; Liu, Z.; Xiong, R.; Pan, C.; Shi, J. Facile synthesis of PANI-modified $CoFe_2O_4$–TiO_2 hierarchical flower-like nanoarchitectures with high photocatalytic activity. *J. Nanopart. Res.* **2013**, *15*, 1643. [CrossRef]
108. Leary, R.; Westwood, A. Carbonaceous nanomaterials for the enhancement of TiO_2 photocatalysis. *Carbon* **2011**, *49*, 741–772. [CrossRef]
109. Woan, K.; Pyrgiotakis, G.; Sigmund, W. Photocatalytic carbon-nanotube–TiO_2 composites. *Adv. Mater.* **2009**, *21*, 2233–2239. [CrossRef]
110. Gui, M.M.; Chai, S.-P.; Xu, B.-Q.; Mohamed, A.R. Enhanced visible light responsive MWCNT/TiO_2 core–shell nanocomposites as the potential photocatalyst for reduction of CO_2 into methane. *Sol. Energy Mater.* **2014**, *122*, 183–189. [CrossRef]
111. Karousis, N.; Tagmatarchis, N.; Tasis, D. Current Progress on the chemical modification of carbon nanotubes. *Chem. Rev.* **2010**, *110*, 5366–5397. [CrossRef] [PubMed]
112. Ismail, A.A.; Geioushy, R.A.; Bouzid, H.; Al-Sayari, S.A.; Al-Hajry, A.; Bahnemann, D.W. TiO_2 decoration of graphene layers for highly efficient photocatalyst: Impact of calcination at different gas atmosphere on photocatalytic efficiency. *Appl. Catal. B* **2013**, *129*, 62–70. [CrossRef]

113. Liu, H.; Lv, T.; Zhu, Z. Template-assisted synthesis of hollow TiO_2@rGO core–shell structural nanospheres with enhanced photocatalytic activity. *J. Mol. Catal. A* **2015**, *404–405*, 178–185. [CrossRef]
114. Zou, R.; Zhang, Z.; Yu, L.; Tian, Q.; Chen, Z.; Hu, J. A general approach for the growth of metal oxide nanorod arrays on graphene sheets and their applications. *Chem. A Eur. J.* **2011**, *17*, 13912–13917. [CrossRef] [PubMed]
115. Liu, J.; Zhu, W.; Yu, S.; Yan, X. Three dimensional carbogenic dots/TiO_2 nanoheterojunctions with enhanced visible light-driven photocatalytic activity. *Carbon* **2014**, *79*, 369–379. [CrossRef]
116. Zeng, X.; Wang, Z.; Meng, N.; McCarthy, D.T.; Deletic, A.; Pan, J.-H.; Zhang, X. Highly dispersed TiO_2 nanocrystals and carbon dots on reduced graphene oxide: Ternary nanocomposites for accelerated photocatalytic water disinfection. *Appl. Catal. B* **2017**, *202*, 33–41. [CrossRef]
117. Tong, Z.; Yang, D.; Xiao, T.; Tian, Y.; Jiang, Z. Biomimetic fabrication of g-C_3N_4/TiO_2 nanosheets with enhanced photocatalytic activity toward organic pollutant degradation. *Chem. Eng. J.* **2015**, *260*, 117–125. [CrossRef]
118. DIRECTIVE 2000/60/EC of the European Parliament and of the Council. Available online: http://ec.europa.eu/health/endocrine_disruptors/docs/wfd_200060ec_directive_en.pdf (accessed on 10 January 2017).
119. Oller, I.; Malato, S.; Sánchez-Pérez, J.A. Combination of advanced oxidation processes and biological treatments for wastewater decontamination—A review. *Sci. Total Environ.* **2011**, *409*, 4141–4166. [CrossRef] [PubMed]
120. Chong, M.N.; Jin, B.; Chow, C.W.K.; Saint, C. Recent developments in photocatalytic water treatment technology: A review. *Water Res.* **2010**, *44*, 2997–3027. [CrossRef] [PubMed]
121. Gaya, U.I.; Abdullah, A.H. Heterogeneous photocatalytic degradation of organic contaminants over titanium dioxide: A review of fundamentals, progress and problems. *J. Photochem. Photobiol. C* **2008**, *9*, 1–12. [CrossRef]
122. Fiorentino, A.; Ferro, G.; Alferez, M.C.; Polo-López, M.I.; Fernández-Ibañez, P.; Rizzo, L. Inactivation and regrowth of multidrug resistant bacteria in urban wastewater after disinfection by solar-driven and chlorination processes. *J. Photochem. Photobiol. B* **2015**, *148*, 43–50. [CrossRef] [PubMed]
123. Malato, S.; Fernández-Ibáñez, P.; Maldonado, M.I.; Blanco, J.; Gernjak, W. Decontamination and disinfection of water by solar photocatalysis: Recent overview and trends. *Catal. Today* **2009**, *147*, 1–59. [CrossRef]
124. Dong, S.; Feng, J.; Fan, M.; Pi, Y.; Hu, L.; Han, X.; Liu, M.; Sun, J.; Sun, J. Recent developments in heterogeneous photocatalytic water treatment using visible light-responsive photocatalysts: A review. *RSC Adv.* **2015**, *5*, 14610–14630. [CrossRef]
125. Kowalska, E.; Wei, Z.; Karabiyik, B.; Herissan, A.; Janczarek, M.; Endo, M.; Markowska-Szczupak, A.; Remita, H.; Ohtani, B. Silver-modified titania with enhanced photocatalytic and antimicrobial properties under UV and visible light irradiation. *Catal. Today* **2015**, *252*, 136–142. [CrossRef]
126. Gao, L.; Gan, W.; Xiao, S.; Zhan, X.; Li, J. A robust superhydrophobic antibacterial Ag–TiO_2 composite film immobilized on wood substrate for photodegradation of phenol under visible-light illumination. *Ceram. Int.* **2016**, *42*, 2170–2179. [CrossRef]
127. Mallakpour, S.; Khadem, E. Carbon nanotube–metal oxide nanocomposites: Fabrication, properties and applications. *Chem. Eng. J.* **2016**, *302*, 344–367. [CrossRef]
128. Yang, J.; Dai, J.; Li, J. Visible-light-induced photocatalytic reduction of Cr(VI) with coupled Bi_2O_3/TiO_2 photocatalyst and the synergistic bisphenol A oxidation. *Environ. Sci. Pollut. Res.* **2013**, *20*, 2435–2447. [CrossRef] [PubMed]
129. Liu, L.; Luo, C.; Xiong, J.; Yang, Z.; Zhang, Y.; Cai, Y.; Gu, H. Reduced graphene oxide (rGO) decorated TiO_2 microspheres for visible-light photocatalytic reduction of Cr(VI). *J. Alloys Compd.* **2017**, *690*, 771–776. [CrossRef]
130. Wang, X.; Zhang, J.; Sun, W.; Yang, W.; Cao, J.; Li, Q.; Peng, Y.; Shang, J.K. Anti-algal activity of palladium oxide-modified nitrogen-doped titanium oxide photocatalyst on *Anabaena* sp. PCC 7120 and its photocatalytic degradation on Microcystin LR under visible light illumination. *Chem. Eng. J.* **2015**, *264*, 437–444. [CrossRef]
131. Wang, S.; Ang, H.M.; Tade, M.O. Volatile organic compounds in indoor environment and photocatalytic oxidation: State of the art. *Environ. Int.* **2007**, *33*, 694–705. [CrossRef] [PubMed]
132. Lasek, J.; Yu, Y.-H.; Wu, J.C.S. Removal of NO_x by photocatalytic processes. *J. Photochem. Photobiol. C* **2013**, *14*, 29–52. [CrossRef]

133. Balbuena, J.; Carraro, G.; Cruz, M.; Gasparotto, A.; Maccato, C.; Pastor, A.; Sada, C.; Barreca, D.; Sanchez, L. Advances in photocatalytic NO_x abatement through the use of Fe_2O_3/TiO_2 nanocomposites. *RSC Adv.* **2016**, *6*, 74878–74885. [CrossRef]
134. Trapalis, A.; Todorova, N.; Giannakopoulou, T.; Boukos, N.; Speliotis, T.; Dimotikali, D.; Yu, J. TiO_2/graphene composite photocatalysts for NO_x removal: A comparison of surfactant-stabilized graphene and reduced graphene oxide. *Appl. Catal. B* **2016**, *180*, 637–647. [CrossRef]
135. Ma, J.; Wang, C.; He, H. Enhanced photocatalytic oxidation of NO over g-C_3N_4-TiO_2 under UV and visible light. *Appl. Catal. B* **2016**, *184*, 28–34. [CrossRef]
136. Xu, M.; Wang, Y.; Geng, J.; Jing, D. Photodecomposition of NO_x on Ag/TiO_2 composite catalysts in a gas phase reactor. *Chem. Eng. J.* **2017**, *307*, 181–188. [CrossRef]
137. Demeestere, K.; Dewulf, J.; Ohno, T.; Salgado, P.H.; van Langenhove, H. Visible light mediated photocatalytic degradation of gaseous trichloroethylene and dimethyl sulfide on modified titanium dioxide. *Appl. Catal. B* **2005**, *61*, 140–149. [CrossRef]
138. Huang, H.; Li, D.; Lin, Q.; Zhang, W.; Shao, Y.; Chen, Y.; Sun, M.; Fu, X. Efficient degradation of benzene over $LaVO_4/TiO_2$ nanocrystalline heterojunction photocatalyst under visible light irradiation. *Environ. Sci. Technol.* **2009**, *43*, 4164–4168. [CrossRef] [PubMed]
139. Xiao, G.; Wang, X.; Li, D.; Fu, X. $InVO_4$-sensitized TiO_2 photocatalysts for efficient air purification with visible light. *J. Photochem. Photobiol. A* **2008**, *193*, 213–221. [CrossRef]
140. Ratova, M.; Kelly, P.J.; West, G.T.; Tosheva, L.; Edge, M. Reactive magnetron sputtering deposition of bismuth tungstate onto titania nanoparticles for enhancing visible light photocatalytic activity. *Appl. Surf. Sci.* **2017**, *392*, 590–597. [CrossRef]
141. Wongaree, M.; Chiarakorn, S.; Chuangchote, S.; Sagawa, T. Photocatalytic performance of electrospun CNT/TiO_2 nanofibers in a simulated air purifier under visible light irradiation. *Environ. Sci. Pollut. Res.* **2016**, *23*, 21395–21406. [CrossRef] [PubMed]
142. Stucchi, M.; Bianchi, C.L.; Pirola, C.; Cerrato, G.; Morandi, S.; Argirusis, C.; Sourkouni, G.; Naldoni, A.; Capucci, V. Copper NPs decorated titania: A novel synthesis by high energy US with a study of the photocatalytic activity under visible light. *Ultrason. Sonochem.* **2016**, *31*, 295–301. [CrossRef] [PubMed]
143. Stucchi, M.; Bianchi, C.L.; Pirola, C.; Vitali, S.; Cerrato, G.; Morandi, S.; Argirusis, C.; Sourkouni, G.; Sakkas, P.M.; Capucci, V. Surface decoration of commercial micro-sized TiO_2 by means of high energy ultrasound: A way to enhance its photocatalytic activity under visible light. *Appl. Catal. B* **2015**, *178*, 124–132. [CrossRef]
144. Ragesh, P.; Anand Ganesh, V.; Nair, S.V.; Nair, A.S. A review on 'self-cleaning and multifunctional materials'. *J. Mater. Chem. A* **2014**, *2*, 14773–14797. [CrossRef]
145. Tian, G.; Chen, Y.; Zhai, R.; Zhou, J.; Zhou, W.; Wang, R.; Pan, K.; Tian, C.; Fu, H. Hierarchical flake-like Bi_2MoO_6/TiO_2 bilayer films for visible-light-induced self-cleaning applications. *J. Mater. Chem. A* **2013**, *1*, 6961–6968. [CrossRef]
146. Banerjee, S.; Dionysiou, D.D.; Pillai, S.C. Self-cleaning applications of TiO_2 by photo-induced hydrophilicity and photocatalysis. *Appl. Catal. B* **2015**, *176–177*, 396–428. [CrossRef]
147. Zhu, Y.F.; Yu, C.F.; Ni, C.Y. Low temperature synthesis and photocatalytic performance of tungsten trioxide film. *Surf. Eng.* **2016**, *32*, 26–31. [CrossRef]
148. Qiu, X.; Miyauchi, M.; Sunada, K.; Minoshima, M.; Liu, M.; Lu, Y.; Li, D.; Shimodaira, Y.; Hosogi, Y.; Kuroda, Y. Hybrid Cu_xO/TiO_2 nanocomposites as risk-reduction materials in indoor environments. *ACS Nano* **2012**, *6*, 1609–1618. [CrossRef] [PubMed]
149. Verbruggen, S.W.; Keulemans, M.; Filippousi, M.; Flahaut, D.; van Tendeloo, G.; Lacombe, S.; Martens, J.A.; Lenaerts, S. Plasmonic gold–silver alloy on TiO_2 photocatalysts with tunable visible light activity. *Appl. Catal. B* **2014**, *156–157*, 116–121. [CrossRef]
150. Long, M.; Zheng, L.; Tan, B.; Shu, H. Photocatalytic self-cleaning cotton fabrics with platinum(IV) chloride modified TiO_2 and N-TiO_2 coatings. *Appl. Surf. Sci.* **2016**, *386*, 434–441. [CrossRef]
151. Wang, R.; Wang, X.; Xin, J.H. Advanced visible-light-driven self-cleaning cotton by $Au/TiO_2/SiO_2$ photocatalysts. *ACS Appl. Mater. Interfaces* **2010**, *2*, 82–85. [CrossRef]
152. Pakdel, E.; Daoud, W.A.; Sun, L.; Wang, X. Visible and UV functionality of TiO_2 ternary nanocomposites on cotton. *Appl. Surf. Sci.* **2014**, *321*, 447–456. [CrossRef]

153. Petronella, F.; Rtimi, S.; Comparelli, R.; Sanjines, R.; Pulgarin, C.; Curri, M.L.; Kiwi, J. Uniform TiO_2/In_2O_3 surface films effective in bacterial inactivation under visible light. *J. Photochem. Photobiol. A* **2014**, *279*, 1–7. [CrossRef]
154. Karimi, L.; Yazdanshenas, M.E.; Khajavi, R.; Rashidi, A.; Mirjalili, M. Using graphene/TiO_2 nanocomposite as a new route for preparation of electroconductive, self-cleaning, antibacterial and antifungal cotton fabric without toxicity. *Cellulose* **2014**, *21*, 3813–3827. [CrossRef]
155. Wu, S.-Y.; Su, S.-K.; Chang, C.-J.; Huang, C.-H.; Chen, J.-K. Sol-gel-synthesized titania-vanadia nanocrystal films for triple-functional window coatings. *Ceram. Int.* **2016**, *42*, 17610–17619. [CrossRef]
156. Lee, J.; Mahendra, S.; Alvarez, P.J.J. Nanomaterials in the construction industry: A review of their applications and environmental health and safety considerations. *ACS Nano* **2010**, *4*, 3580–3590. [CrossRef] [PubMed]
157. Spitzmiller, M.; Mahendra, S.; Damoiseaux, R. *Nanotechnology in Eco-Efficient Construction*; Woodhead Publishing: Sawston, UK, 2013; pp. 127–158.
158. Torgal, F.P.; Jalali, S. Nanotechnology: Advantages and drawbacks in the field of construction and building materials. *Constr. Build. Mater.* **2011**, *25*, 582–590. [CrossRef]
159. Macphee, D.E.; Folli, A. Photocatalytic concretes—The interface between photocatalysis and cement chemistry. *Cem. Concr. Res.* **2016**, *85*, 48–54. [CrossRef]
160. Chen, J.; Poon, C.-S. Photocatalytic construction and building materials: From fundamentals to applications. *Build. Environ.* **2009**, *44*, 1899–1906. [CrossRef]
161. Franzoni, E.; Fregni, A.; Gabrielli, R.; Graziani, G.; Sassoni, E. Compatibility of photocatalytic TiO_2-based finishing for renders in architectural restoration: A preliminary study. *Build. Environ.* **2014**, *80*, 125–135. [CrossRef]
162. Bergamonti, L.; Alfieri, I.; Franzò, M.; Lorenzi, A.; Montenero, A.; Predieri, G.; Raganato, M.; Calia, A.; Lazzarini, L.; Bersani, D.; et al. Synthesis and characterization of nanocrystalline TiO_2 with application as photoactive coating on stones. *Environ. Sci. Pollut. Res.* **2014**, *21*, 13264–13277. [CrossRef] [PubMed]
163. Pinho, L.; Rojas, M.; Mosquera, M.J. Ag–SiO_2–TiO_2 nanocomposite coatings with enhanced photoactivity for self-cleaning application on building materials. *Appl. Catal. B* **2015**, *178*, 144–154. [CrossRef]
164. Guo, M.-Z.; Maury-Ramirez, A.; Poon, C.S. Photocatalytic activities of titanium dioxide incorporated architectural mortars: Effects of weathering and activation light. *Build. Environ.* **2015**, *94*, 395–402. [CrossRef]
165. Janus, M.; Zatorska, J.; Czyżewski, A.; Bubacz, K.; Kusiak-Nejman, E.; Morawski, A.W. Self-cleaning properties of cement plates loaded with N,C-modified TiO_2 photocatalysts. *Appl. Surf. Sci.* **2015**, *330*, 200–206. [CrossRef]